COPY 3

UCRL- 1382

UNCLA

UNIVERSITY OF CALIFORNIA — BERKELEY

TWO-WEEK LOAN COPY

This is a Library Circulating Copy which may be borrowed for two weeks. For a personal retention copy, call Tech. Info. Division, Ext. 5545

RADIATION LABORATORY

DISCLAIMER

This document was prepared as an account of work sponsored by the United States Government. While this document is believed to contain correct information, neither the United States Government nor any agency thereof, nor the Regents of the University of California, nor any of their employees, makes any warranty, express or implied, or assumes any legal responsibility for the accuracy, completeness, or usefulness of any information, apparatus, product, or process disclosed, or represents that its use would not infringe privately owned rights. Reference herein to any specific commercial product, process, or service by its trade name, trademark, manufacturer, or otherwise, does not necessarily constitute or imply its endorsement, recommendation, or favoring by the United States Government or any agency thereof, or the Regents of the University of California. The views and opinions of authors expressed herein do not necessarily state or reflect those of the United States Government or any agency thereof or the Regents of the University of California.

UCRL-1382
Unclassified - Physics Distribution

UNIVERSITY OF CALIFORNIA

Radiation Laboratory

Contract No. W-7405-eng-48

I. THE SCATTERING OF HIGH ENERGY NEUTRONS BY NUCLEI

II. LATERAL SPREAD OF PARTICLES IN CASCADE SHOWERS

Sidney Fernbach

(Thesis)

July 2, 1951

Berkeley, California

CONTENTS

		Page
I.	The Scattering of High Energy Neutrons by Nuclei	3
	1. Introduction	3
	2. Calculations	4
	3. Comparison of Theory with Experimental Data	13
	(a) 90 Mev Data	13
	(b) 280 Mev Data	16
	4. Conclusions	18
	References	20
	Figures	21
II.	Lateral Spread of Particles in Cascade Showers	30
	1. Introduction	30
	2. Reconstruction of a Function from a Finite Number of its Moments	32
	3. Moments of the Distribution Function in Showers	35
	(a) Approximation A	35
	(b) Asymptotic Expansions for the Moments	42
	4. Moments of the Distribution Functions as a Function of Shower Depth (Approximation A)	49
	5. The Distribution Functions	55
	(a) Approximation A	55
	(b) Effect of Collision Loss	59
	(c) Distribution Functions at other Shower Depths	61
	References	63
	Tables	64
	Figures	80
	Acknowledgments	90

I. The Scattering of High Energy Neutrons by Nuclei

1. INTRODUCTION

Results obtained from experiments on scattering of neutrons are valuable in the study of nuclear structure. With the aid of various models representing the nucleus it is possible to build up a consistent scheme, whereby all nuclei can be described in terms of a limited number of parameters. Low energy scattering is characterized by series of resonances. As the energies increases up to approximately 1 Mev, the cross sections, especially for the heavy elements, level off. The neutron wave length becomes smaller than the radius and we approach the classical region where the total cross section should be $2\pi R^2$. At still higher energies the wave length of the neutrons becomes small compared to the radius and the nucleus becomes somewhat transparent. This partial transparency was discussed by Serber[1], who pointed out that at 100 Mev the scattering mean free path becomes comparable with the nuclear radius.

The first very high energy experiments were performed by Cook, McMillan, Peterson, and Sewell[2] with neutrons having energies in the vicinity of 90 Mev. To explain the results obtained the model described in this paper was devised. It represents nuclear matter as having a mean free path for scattering neutrons such as suggested by Serber. It also turns out that nuclear matter must be characterized by an index of refraction as well. Thus all

nuclei are treated as spheres of uniform density having a refractive index and absorption coefficient, differing from each other in size only. Such a model may be referred to as an "optical" or "transparent" model of the nucleus.

In the following section we shall set up and calculate the cross sections from the "optical" model. Then, in section 3 we shall compare the results obtained from the calculation with existing experimental data.

2. CALCULATIONS

Nuclear data obtained from experiments at lower energies show that the volume of a nucleus depends upon the number of particles contained in it. This leads to the relationship

$$R = r_o A^{1/3}$$

for the radius of a nucleus. r_o has been determined in many ways, one of these being from experiments on the scattering of neutrons. In the low Mev region it turns out that the nucleus is quite opaque and absorptive with a sticking probability of unity for incident particles. In this region, scattering experiments have been performed by Grahame and Seaborg[3] at 7 Mev, Amaldi et al[4] at 14 Mev and Sherr[5] at 25 Mev. From the results obtained, the radii of the various target nuclei can be calculated since an opaque sphere theoretically shows a total cross section of $2\pi R^2$. If for example, one calculates R from Amaldi's

data one finds $R = (1.22 + 1.37\ A^{1/3}) \times 10^{-13}$ cm. The intercept can then be thought of as being somehow related to the wave length of the incident particle. As the incident energy increases this wave length becomes smaller and for high enough energies will be small compared to the radius of the nucleus. In such a case then one can neglect the intercept and find a straight line R vs. $A^{1/3}$ which goes thru the origin. In the transparent model, the energy is considered high enough for this assumption. As a matter of fact, this model is a high energy approximation and explicitly demands that $\lambda\!\!\!^{-} \ll R$, that is, the wavelength of the incoming particle be small compared to the radius of the nucleus.

The nucleus is to be represented by a sphere of constant density with an absorption coefficient and an index of refraction. These constants are calculable from known experimental data if one assumes the Fermi description of the nucleus. The differential and total cross sections can then be calculated by using the WKB approximation; this being applicable because the wave length of the incident particle is small enough compared to the radius of the scattering center to make the problem almost classical.

If $k = \left(2ME/\hbar^2\right)^{1/2}$ is the propagation vector of the incident wave outside the nucleus, its propagation vector inside is increased by k_1 such that $k + k_1 = \left[2M\,(E + V)/\hbar^2\right]^{1/2}$. It follows then that

$$k_1 = k\left[\left(1 + \frac{V}{E}\right)^{\frac{1}{2}} - 1\right] . \qquad (1)$$

Using $R = 1.37\ A^{1/3} \times 10^{-13}$ cm as deduced by Cook et al from the data of Amaldi et al and Sherr, one obtains a Fermi energy of 22 Mev. The potential is usually taken to be about 8 Mev above the Fermi energy, so $V = 30$ Mev. The high energy experiments of Cook et al were done at approximately 90 Mev, for which $k = 2.08 \times 10^{13}\ \mathrm{cm}^{-1}$. Using these values, we get $k_1 = 3.22 \times 10^{12}\ \mathrm{cm}^{-1}$. The absorption coefficient in nuclear matter is found from the product of the particle density and cross section for scattering of the neutron by a particle in the nucleus:

$$K = \frac{3A\sigma}{4\pi R^3} \quad . \qquad (2)$$

In terms of the n-p and n-n cross sections $\sigma = \left[Z\sigma_{np} + (A - Z)\sigma_{nn}\right]/A$. Cook et al give for the scattering of a 90 Mev neutron by a free proton $\sigma_{np(free)} = 8.3 \times 10^{-26}\ \mathrm{cm}^2$. This cross section must be reduced to allow for the effect of the exclusion principle on the scattering by a proton bound in the nucleus. According to Goldberger[6], the factor is $\sigma_{np} = \frac{2}{3}\sigma_{np(free)}$. Assuming a 1/E dependence of the cross section we find, for $E = 90 + 30 = 120$ Mev, $\sigma_{np} = 4.15 \times 10^{-26}\ \mathrm{cm}^2$. If, following Goldberger, we take $\sigma_{nn} = \frac{1}{4}\sigma_{np}$, and use the previously quoted radius formula, we obtain $K = 2.4 \times 10^{12}\ \mathrm{cm}^{-1}$ for $Z/A = \frac{1}{2}$. However, measured values of the p-p cross section at 100 Mev[7] indicate that σ_{nn} is almost equal to σ_{np}. If we assume that $\sigma_{nn} = \frac{3}{4}\sigma_{np}$, we obtain $K = 3.3 \times 10^{12}\ \mathrm{cm}^{-1}$. This value will not vary much with Z/A because

of the near equality of σ_{nn} and σ_{np}. In the ensuing calculation we shall assume that $kR \gg 1$, $\frac{k_1}{k}$ and $\frac{K}{k} \ll 1$ so that k_1R and KR are of order one. At energies higher than 90 Mev, it is evident that these conditions will be more valid.

The scattering cross section consists of two parts. The first, the "absorption cross section" is just πR^2 times the probability that a neutron collides with a particle in the nucleus. This is not true absorption: inelastic scattering and scattering with exchange are included. The second part, the "diffraction" or "shadow" scattering, is elastic scattering arising from the distrubance of the incident plane waves by the nucleus. The calculation is readily done by applying the WKB approximation to a square potential well with complex propagation constant inside and finding the phase shifts for the various partial waves. Before doing this, however, it is instructive to see that the same results can be obtained from an optical model. To illustrate the calculation, we first consider the scattering from a disc in which k_1 and K rise to their interior values in a distance larger than $1/k$. Then one may neglect scattering at the surfaces and, for unit amplitude of incident waves, the wave transmitted through the disc will have an amplitude and relative phase $a = \exp(-\frac{1}{2}K + ik_1)T$. The absorption cross section is

$$\sigma_a = \pi R^2(1 - |a|^2) = \pi R^2(1 - e^{-KT}) \quad . \qquad (3)$$

The diffraction cross section can be found from the consideration that on a plane behind the disc the wave is no longer plane, but differs from a plane wave by an amplitude $(1 - a)$ in the shadow of the disc. This amplitude represents a scattered wave, and the corresponding cross section is

$$\sigma_d = \pi R^2 \left| 1 - a \right|^2 = \pi R^2 \left(1 - 2e^{-\frac{1}{2}KT} \cos k_1 T + e^{-KT}\right) . \tag{4}$$

The absorption cross section is, of course, always less than πR^2, but the diffraction cross section may be either larger or smaller, depending on the magnitude of the phase shift. For large KT, $\sigma_a = \sigma_d = \pi R^2$. In the opposite limit of small KT and $k_1 T$

$$\sigma_a = \pi R^2 KT = A\sigma \tag{5}$$

$$\sigma_d = \pi R^2 \left(\tfrac{1}{2}K + k_1\right) T = \tfrac{1}{2} A\sigma \left[1 + 4 \frac{k_1^2}{K^2}\right] KT . \tag{6}$$

Thus for low density or small thickness σ_a approaches the sum of the scattering cross sections of the separate nucleons. The diffraction cross section, however, vanishes in the limit, being proportional to the probability of double scattering.

The corresponding calculations for a sphere are only slightly more complicated. The portion of the wave which strikes the sphere at a distance ρ from a line through the center of the sphere

emerges after traveling a distance 2S, with $S^2 = R^2 - \rho^2$. Its amplitude on emerging is $a = \exp(-K + 2ik_1)S$, so that, in place of (1) we have

$$\sigma_a = 2\pi\int_0^R (1 - e^{-2KS})\rho\, d\rho = 2\pi\int_0^R (1 - e^{-2KS})S\, dS$$

$$= \pi R^2 \left\{ 1 - \left[1 - (1 + 2KR)e^{-2KR} \right] / 2K^2R^2 \right\} . \tag{7}$$

This formula for the absorption cross section has previously been given by Bethe[8]. Similarly in place of (4), we have

$$\sigma_d = 2\pi\int_0^R \left| 1 - e^{(-K + 2ik_1)S} \right|^2 \rho\, d\rho$$

$$= \pi R^2 \Bigg\{ 1 + (1/2\, K^2R^2) \left[1 - (1 + 2KR)e^{-2KR} \right]$$

$$- (1/(\tfrac{1}{4}K^2 + k_1^2)^2 R^2) \Bigg[(\tfrac{1}{4}K^2 - k_1^2)$$

$$+ e^{-KR}\left[2k_1R(\tfrac{1}{4}K^2 + k_1^2) + k_1K \right] \sin 2k_1R$$

$$- e^{-KR}\left[(\tfrac{1}{4}K^2 - k_1^2) + KR(\tfrac{1}{4}K^2 + k_1^2) \right] \cos 2k_1R \Bigg] \Bigg\} . \tag{8}$$

Here we have neglected refraction at the surface of the sphere. This is legitimate since it gives a second order effect, that is,

of order $(k_1/k)k_1R$.

The angular distribution can be obtained similarly but we shall write it in terms of the WKB approximation applied to a partial wave analysis of the scattering. Our problem is to solve

$$\left[\Delta + k'^2 - \frac{\ell(\ell+1)}{r^2}\right] u_\ell(r) = 0 \tag{9}$$

where $k' = k$ for $r > R$

$k' = k + k_1 + \frac{iK}{2}$ for $r < R$.

The phase shifts are easily obtained for the ℓth partial wave, using Langer's[9] expression

$$\delta_\ell = \lim_{r \to \infty} \int_{(r)_o}^{\infty} \sqrt{k'^2 - \frac{(\ell+\frac{1}{2})^2}{r^2}}\, dr - kr + (\ell+\tfrac{1}{2})\,\pi/2 \tag{10}$$

where $(r)_o$ is the zero of the integrand. We assume that K/k and $k_1/k \ll 1$ and integrate out the real axis after expanding the square root in the integrand.

$$\delta_\ell = \alpha_\ell + i\beta_\ell$$

$$= \lim_{r \to \infty} \int_{(r)_o}^{R} \sqrt{k^2 - \frac{(\ell+\frac{1}{2})^2}{r^2}} \left[1 + \frac{(k_1 + \frac{iK}{2})\,k}{k^2 - \frac{(\ell+\frac{1}{2})^2}{r^2}}\right] dr$$

$$+ \int_R^{\infty} \sqrt{k^2 - \frac{(\ell+\frac{1}{2})^2}{r^2}}\, dr - kr + (\ell+\tfrac{1}{2})\,\frac{\pi}{2}$$

$$= \frac{k_1 + \frac{iK}{2}}{k} \sqrt{k^2R^2 - (\ell + \tfrac{1}{2})^2} \tag{11}$$

The absorption cross section is given by the usual expression in partial wave treatment of scattering problems:

$$\sigma_a = \frac{\pi}{k^2} \sum_{\ell} (2\ell+1)\,(1 - e^{-4\beta_\ell}) \tag{12}$$

This leads exactly to equation (7) if we convert the sum in equation (12) to an integral and integrate over $d\ell$, taking as an upper limit $\ell < kR - \frac{1}{2}$. Similarly

$$\sigma_d = \frac{\pi}{k^2} \sum_{\ell} (2\ell+1) \left| 1 - e^{-2i\delta_\ell} \right|^2 \tag{13}$$

gives the σ_d as in equation (8). The differential cross section per unit solid angle can be obtained from the differential scattering amplitude

$$f(\theta) = \frac{1}{2ik} \sum_{\ell} (2\ell+1)(1 - e^{-2i\delta_\ell})\; P_\ell(\cos\theta)$$

through $\sigma(\theta) = \left| f(\theta) \right|^2$. Generally, the sum has to be carried out explicitly at each angle; only in the forward direction is it easily possible to obtain an analytic expression. One can, of course, also replace the sum by an integral and $P_\ell(\cos\theta)$ by $J_0\left[(\ell+\frac{1}{2})\theta\right]$, valid for small angles and large ℓ, then

integrate numerically to obtain $f(\theta)$. If the integral expression is used at zero degrees, we obtain:

$$f(0) = \frac{1}{ik}\int_0^{kR} u\left(e^{2i\alpha u} - 1\right) du \tag{11}$$

where

$$u^2 = k^2 r^2 - (\ell + \tfrac{1}{2})^2 , \tag{12}$$

and

$$\alpha = \frac{2i}{k}\left(k_1 + \frac{iK}{2}\right) .$$

The integration yields

$$f(0) = \frac{1}{ik}\left[-\frac{k^2R^2}{2} - \frac{k^2\left(k_1 - \frac{iK}{2}\right)^2}{4\left(k_1^2 + \frac{K^2}{4}\right)^2} + \frac{k^2\left(k_1 - \frac{iK}{2}\right)^2}{4\left(k_1^2 + \frac{K^2}{4}\right)^2} e^{-KR + i2k_1R}\left(1 + KR - 2ik_1R\right)\right] \tag{15}$$

This equation can be written more simply in terms of the spherical Hankel function of the first kind; $h_1^{(1)}$:

$$f(0) = \frac{kR^2}{2}\left[1 + \frac{2}{\rho^2} + 2ih_1^{(1)}(\rho)\right] \tag{16}$$

where

$$\rho = -(2k_1 + iK)R .$$

It is also possible to make a series expansion for the integral[10], but the series converges very slowly and is not as useful as the sum indicated above.

3. COMPARISON OF THEORY WITH EXPERIMENTAL DATA

(a) 90 Mev Data

For the 90 Mev neutrons we have shown that for a potential depth of 30 Mev, $k_1 = 3.22 \times 10^{12}\ cm^{-1}$ and that K might be between $2.4 \times 10^{12} cm^{-1}$ and $3.3 \times 10^{12} cm^{-1}$ depending on the relative values of σ_{nn} and σ_{np}. We find that these values are consistent with experimental data if we take $R = 1.39\ A^{1/3} \times 10^{-13} cm$ for $k_1R/KR = 1.1$. Thus we adopt the values $k_1 = 3.3 \times 10^{12} cm^{-1}$ ($V = 30.8$ Mev) and $K = 3.0 \times 10^{12}\ cm^{-1}$, corresponding to a mean free path in nuclear matter of $3.3 \times 10^{-13} cm$. In Fig. 1 we have plotted $\sigma_a/\pi R^2$, $\sigma_d/\pi R^2$ and $\sigma_t/\pi R^2 = (\sigma_a + \sigma_d)/\pi R^2$ as functions of KR for the above values of K and k_1. It should be noted that $\sigma_a/\pi R^2$ is a function of KR alone, but that $\sigma_d/\pi R^2$ depends on KR and the ratio k_1R/KR. Fig. 2 shows how σ_t/R^2 varies with the choice of k_1R/KR as a function of k_1R (actually R since k_1 is taken to be $3.3 \times 10^{13} cm^{-1}$ for this plot). It can be seen that for large ratios the cross section may go much higher than the limit of $2\pi R^2$ obtained in the case of the opaque nucleus.

The values of R calculated from the experimental data of Cook et al by use of equations (7) and (8) are shown in Fig. 3

along the line $R = 1.39 \times 10^{-13} A^{1/3}$ cm. The fit is exceptionally good. Further experimental cross sections were measured by DeJuren and Knable[10] at a slightly higher energy, namely 95 Mev. Here again, a good fit of experimental data with an $r_o = 1.38 \times 10^{-13}$cm is obtained.

The question now arises as to the accuracy with which the constants K and k_1 are determined by the scattering data. If k_1 is decreased, keeping K constant, it is found that the radius curve, Fig. 3 is pulled up in the middle; the resultant curve can be approximated by two straight lines, the light elements lying on a steeper line thru the origin, while the heavy elements lie on a less steep line with a positive intercept. Increasing k_1 has the opposite effect. A variation in k_1 of $\pm 0.2 \times 10^{12}$cm^{-1}, or in V of ± 2 Mev, begins to produce appreciable bending. A reduction in K, with fixed k_1, introduces a curvature in the radius line, the center being pulled down and the two ends raised. The curvature becomes noticeable if K is reduced to less than $K = 1.9 \times 10^{12}$cm^{-1}, however K can be almost doubled before the opposite curvature becomes very pronounced.

The total cross section measurements thus determine the index of refraction fairly well, but are quite insensitive to the absorption coefficient. Measurements of σ_a and of the differential diffraction scattering are required for a better evaluation of K. These have been measured experimentally at approximately 90 Mev[11] and the agreement obtained with the constants

assumed above found to be reasonably good. In Fig. 4 we see the comparison between the theoretical results for the ratio σ_a/σ_t and the measured values obtained from attenuation data in a poor geometry experiment. Since the absorption cross section depends only on K and not on k_1, the indications are that $K = 3.0 \times 10^{12}$ cm^{-1} is a fairly good measure of the absorption coefficient. Note that the ratio $\sigma_a/\sigma_t < .5$ in this case. If the nucleus were completely opaque $\sigma_a/\sigma_t = .5$. Similar agreement was obtained in the analysis of absorption cross sections measured by DeJuren and Knable[12].

The comparison between the experimental and calculated differential cross sections for aluminum, copper, and lead are shown in Fig. 5. The theoretical curves were obtained by summing the partial waves as given in equation (14) using the constants which best fit the total cross sections. The experimental points are seen to lie high in the forward direction, but fit fairly well at larger angles. The reason this does not make the theoretical total cross sections too low is that the integral over all angles is weighted by the sine factor, thus giving a negligible contribution for small angles. The opaque model of the nucleus actually gives a higher cross section in the forward direction than does the transparent model, but does not fit so well at larger angles. In shape, the two models give very similar diffraction patterns, at least up to the first minimum. This is especially true for heavy nuclei, as can be seen in Fig. 6. Here

the diffraction patterns calculated for various transparent nuclei are compared with the opaque nucleus, all normalized to unity in the forward direction. The curves for the heaviest nuclei are just about indistinguishable. For the lighter nuclei, the form of the curve is closely the same, but with an altered scale of abscissa, corresponding to using an effective radius somewhat smaller than the true radius. The increase in the half width of the diffraction peak is zero for lead (KR = 1.78), 3.7% for copper (KR = 1.20), 6.2% for aluminum (KR = 0.90), and 9.6% for beryllium (KR = 0.63).

(b) 280 Mev Data

At energies higher than 90 Mev, only total cross sections are known. Fox et al[13] have measured these at 270 Mev, DeJuren[14] at 280 Mev. Also DeJuren and Moyer[15] have studied the variation of total cross section of several elements with energy, the energies ranging from 95 Mev to 280 Mev. The constants K and k_1 can be calculated in a manner similar to that used for the 90 Mev data. It turns out, however, that the best fit to the experimental data is obtained with $k_1 = 0$. This seems surprising since it implies an index of refraction equal to unity, or from equation (1) an effective potential of zero. One can calculate the index of refraction in a different manner than that used here and obtain an expression in terms of the forward scattering amplitudes for the n-n and n-p interactions. Jastrow[16] has done this using both his own hard core model of the nucleon[17] and the

model proposed by Christian and Hart[18] for the n-p interaction and Christian and Noyes[19] for the n-n (actually p-p) interaction. It turns out, indeed, that the hard core model predicts a rapid decrease in the index of refraction and that k_1 does go to zero, being quite small even at 160 Mev. The other model also predicts a decrease but not so rapid as that of Jastrow's. Experimentally the σ vs. E curves show a rather flat cross section below 40 Mev, a rapid decrease that takes place roughly in the next 120 Mev and a flattening off again beyond 160 Mev.

If we take, then, $k_1 = 0$ at 270 - 280 Mev we must still calculate K and see whether this is consistent with the experimental results. Both the n-p and p-p cross sections are known at these high energies and are found to be roughly equal. K calculated from these values ($\sigma_{np} = 3.5$ millbarns at 280 Mev) turns out to be of the order of $2.8 \times 10^{12} cm^{-1}$, when one allows a 10% correction for exclusion effects. The best fit of theoretical and experimental data, however, gives a $K = 2.5 \times 10^{12} cm^{-1}$. The radii calculated with this value of K and $k_1 = 0$ are compared with the best radius curve for the 90 Mev data in Fig. 7. The agreement here is not as good as at 90 Mev, but is not too unreasonable. The large radii lie below and the small radii above the curve. Since, for $k_1 = 0$, the total cross section is very sensitive to K, it may be that the densities of the light and heavy nuclei do differ somewhat. The model proposed here, however, is a statistical model and should fit the heavy nuclei much better

10^{12} ?

than the light ones. Thus if one ignores the light nuclei, one finds that a $K = 2.3 \times 10^{13} cm^{-1}$ combined with $k_1 = 0$ and $r_o = 1.39 \times 10^{-13}$ cm fits the nuclei heavier than copper very well. It should be mentioned that at these high energies the absorption cross section makes up a large fraction of the total cross section. This is seen in Fig. 8 where $\sigma_a/\pi R^2$ and $\sigma_t/\pi R^2$ are plotted for the case $k_1 = 0$. DeJuren[14] has measured a lower limit on σ_a/σ_t and has found it to be 0.5. Recent unpublished results[20], however show that the actual ratio may be much higher, in agreement with the transparent model.

4. CONCLUSIONS

The scattering high energy neutrons by complex nuclei can be described reasonably well by a simple optical model for the nucleus. This model assigns a common index of refraction and mean free path for absorption to all nuclei, these constants varying with energy, the former rapidly decreasing, the latter slowly increasing. The distinguishing feature of different nuclei, then, is size. With reasonable accuracy the radius of the nucleus can be taken to be $1.39\ A^{1/3} \times 10^{-13}$ cm.

This model represents a high energy approximation and does not describe the scattering of neutrons with energy much below 90 Mev. For example, at 42 Mev, the next lower energy for which scattering data is available, is already out of the region of validity. At this energy kR is not large compared with k_1R

and KR. Also at this energy the boundary conditions require more thorough investigation, since one begins to get into a region where the radius curve may have a finite intercept.

No definite conclusions can be drawn concerning the fit to the highest energy data available, namely 270 - 280 Mev, until more information is available concerning the relative magnitude of the absorption and total cross sections and diffraction scattering.

REFERENCES

1. R. Serber, Phys. Rev. 72, 1114 (1947).

2. L. J. Cook, E. M. McMillan, J. M. Peterson, and D. C. Sewell, Phys. Rev. 75, 7 (1949).

3. D. C. Grahame and G. T. Seaborg, Phys. Rev. 53, 795 (1938).

4. E. Amaldi, D. Bocciarelli, B. N. Cacciapuoti, and G. C. Trabacchi, Nuovo Cimento 3, 203 (1946).

5. R. Sherr, Phys. Rev. 68, 240 (1945).

6. M. L. Goldberger, Phys. Rev. 74, 1269 (1948).

7. R. W. Birge, Phys. Rev. 80, 490 (1950).

8. H. A. Bethe, Phys. Rev. 57, 1125 (1940).

9. R. E. Langer, Phys. Rev. 51, 669 (1937).

10. H. C. Van de Hulst, Recherches Astronomiques des l'Observatoire d'Utrecht XI, Part 1 (1946).

11. A. Bratenahl, S. Fernbach, R. H. Hildebrand, C. E. Leith, and B. J. Moyer, Phys. Rev. 77, 597 (1950).

12. J. DeJuren and N. Knable, Phys. Rev. 77, 606 (1950).

13. R. Fox, C. Leith, L. Wouters, and K. R. MacKenzie, Phys. Rev. 80, 23 (1950).

14. James DeJuren, Phys. Rev. 80, 27 (1950).

15. J. DeJuren and B. J. Moyer, Phys. Rev. 81, 919 (1951).

16. Robert Jastrow, Phys. Rev. 82, 261 (1951).

17. R. Jastrow, Phys. Rev. 81, 165 (1951).

18. R. S. Christian and E. W. Hart, Phys. Rev. 77, 441 (1950).

19. R. S. Christian and H. P. Noyes, Phys. Rev. 79, 85 (1950).

20. W. P. Ball, unpublished results.

FIGURE CAPTIONS

Figure 1. $\sigma_a/\pi R^2$, $\sigma_d/\pi R^2$, and $\sigma_t/\pi R^2$ as a function of KR for $k_1 = 3.3 \times 10^{12} cm^{-1}$.

Figure 2. $\sigma_t/\pi R^2$ for various ratios k_1R/KR as a function of k_1R.

Figure 3. Nuclear radius vs. $A^{1/3}$ calculated for 90 Mev data.

Figure 4. Ratio of absorption cross section to total cross section as a function of radius.

Figure 5. Comparison of theoretical angular distributions for aluminum, copper, and lead with experimental data.

Figure 6. Comparison of shapes of diffraction patterns of transparent nucleus with that of opaque nucleus.

Figure 7. Nuclear radius vs. $A^{1/3}$ calculated for 280 Mev data.

Figure 8. $\sigma_a/\pi R^2$ and $\sigma_t/\pi R^2$ as a function of KR for $k_1 = 0$.

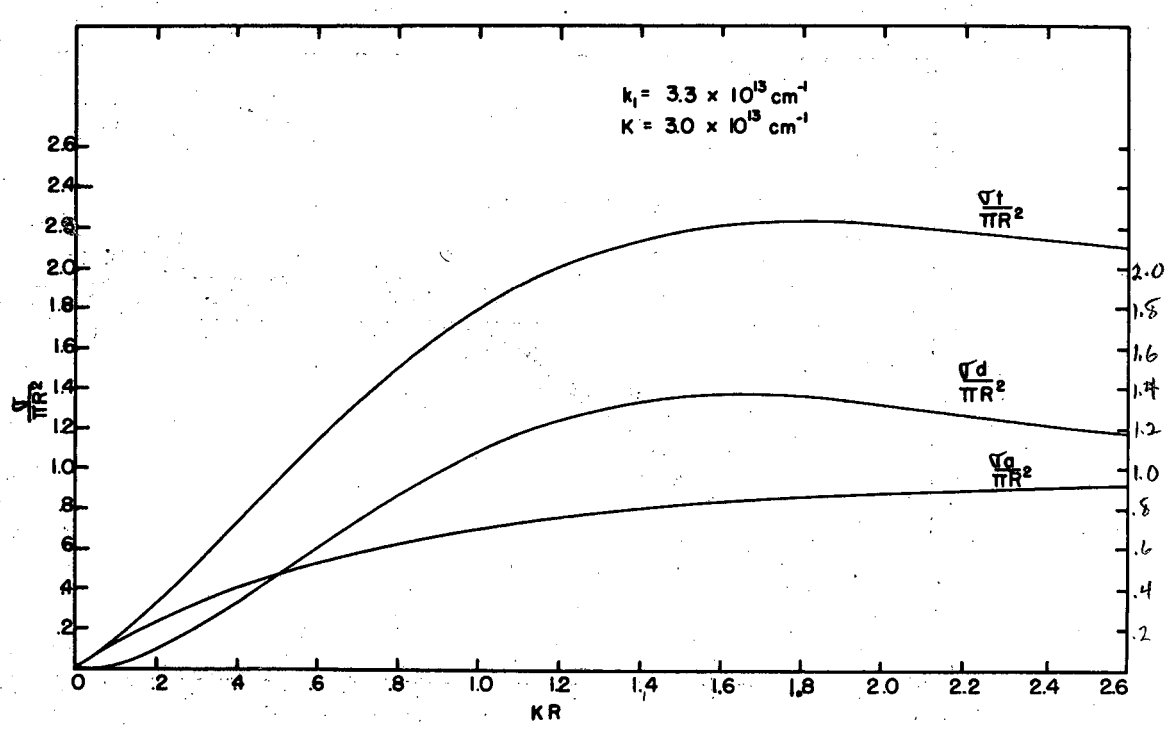

FIG. 1 – SECTION I

MU 2075

178471

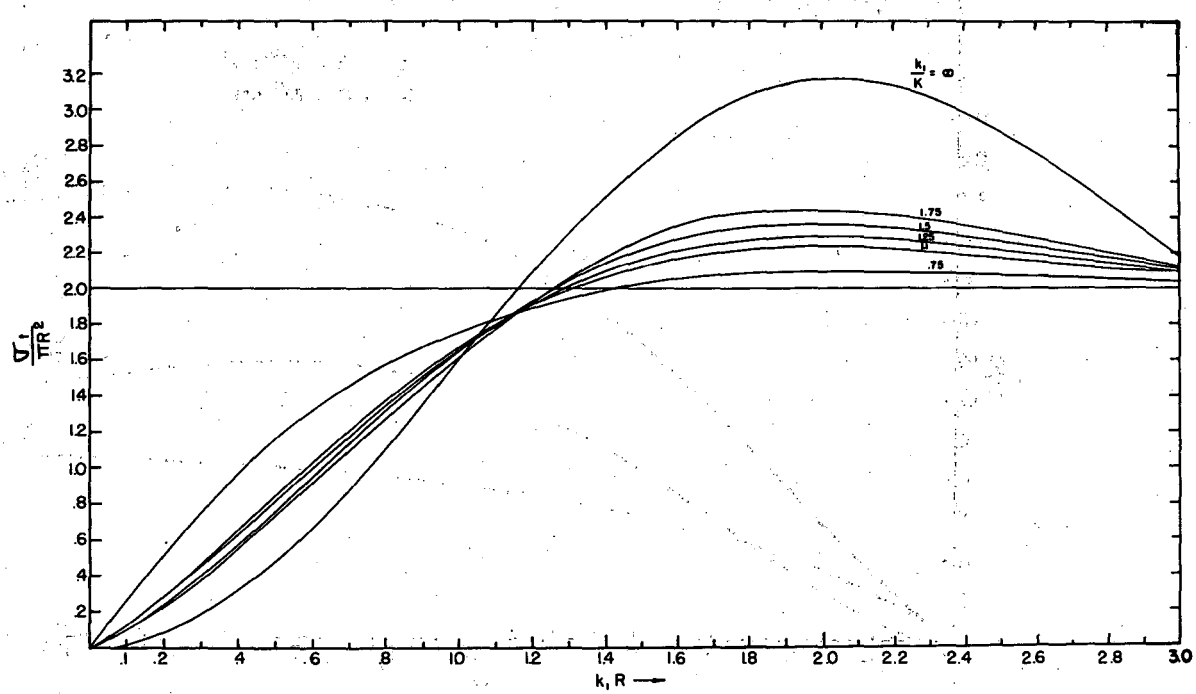

FIG. 2 – SECTION I

MU 2076

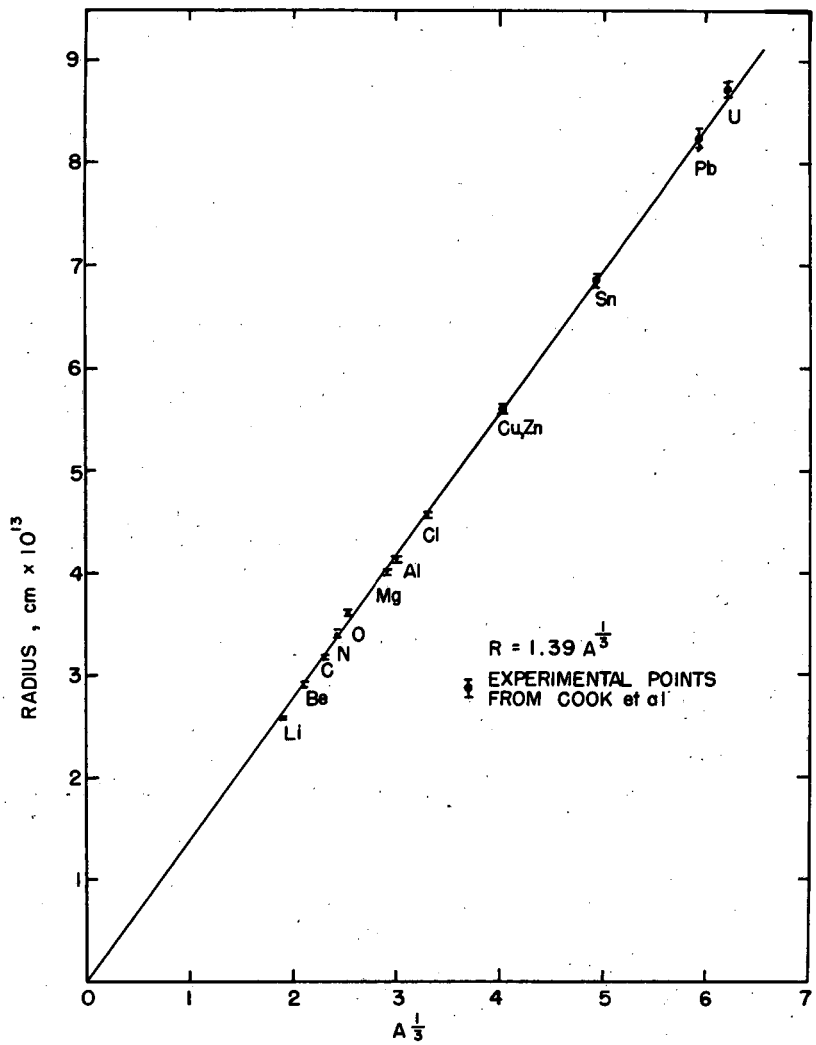

FIG. 3 - SECTION I

MU 2-077

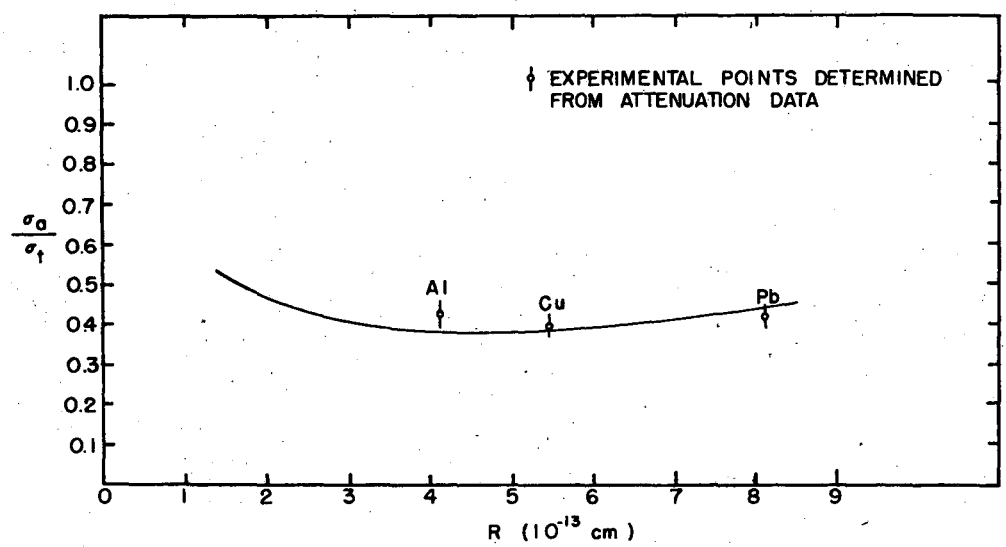

FIG. 4 - SECTION I

$K = 3.0 \times 10^{12}\ cm^{-1}$, $k_1 = 3.3 \times 10^{12} cm^{-1}$

MU 2078

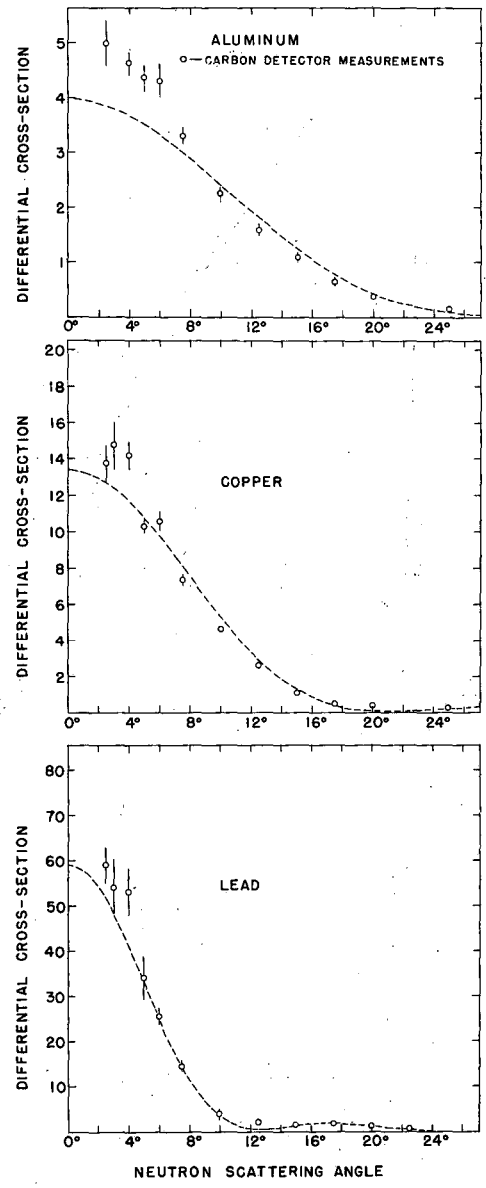

FIG. 5 — SECTION I

MU 1494 A

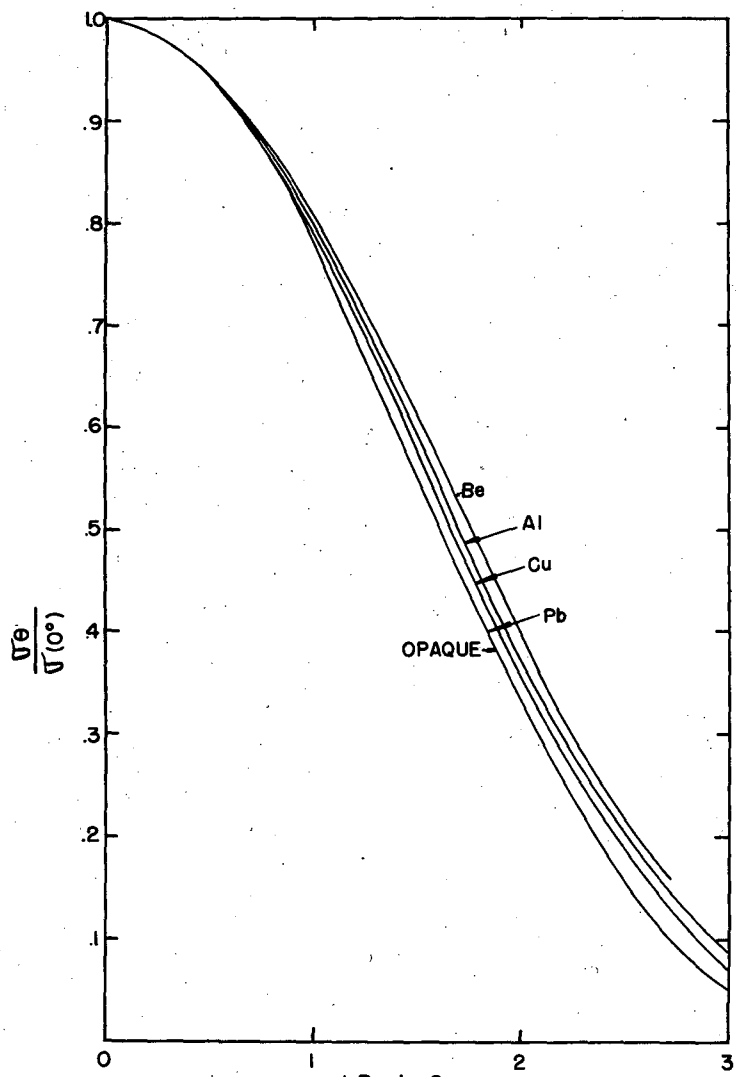

FIG. 6 - SECTION I

MU 2079

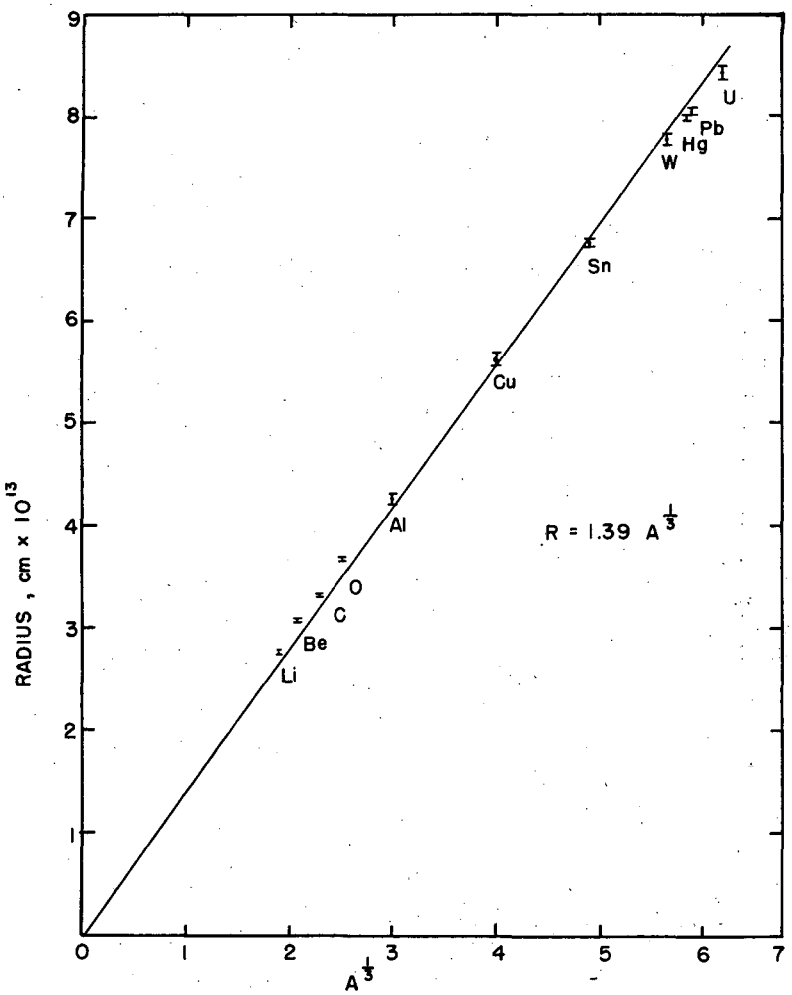

FIG. 7 - SECTION I

MU 2080

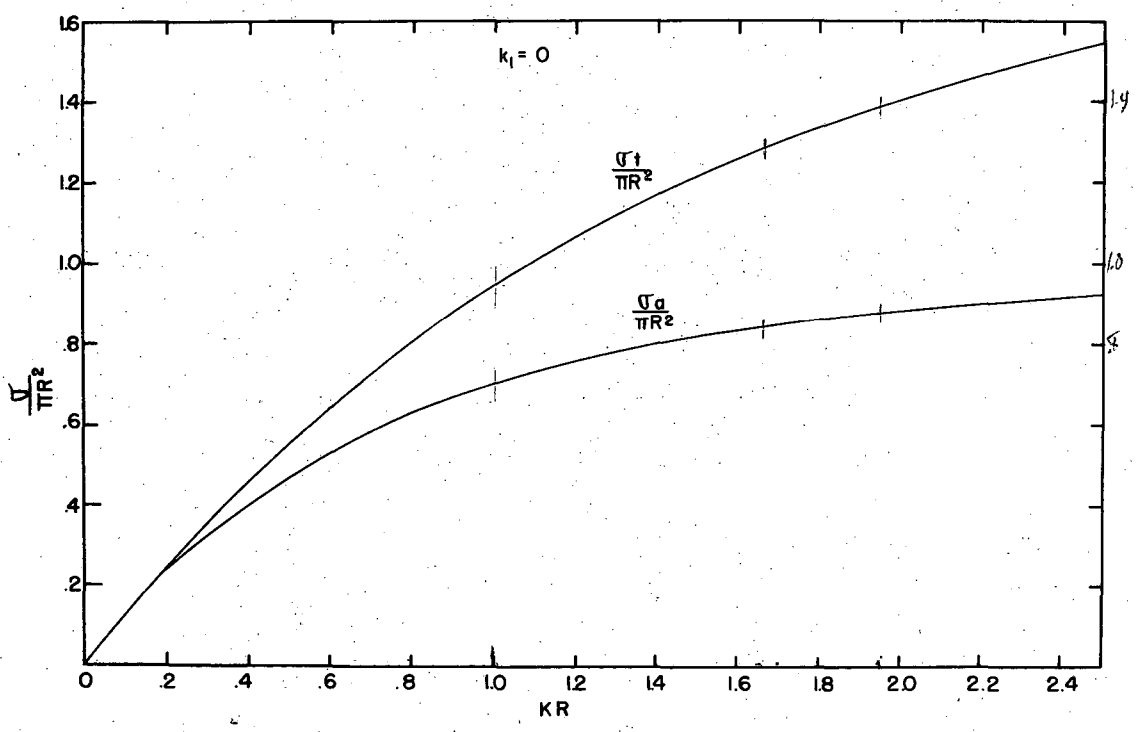

FIG. 8 - SECTION I

MU 2081
178601

S. Fernbach, thesis UCRL - 1382

Fernbach, Serber, Taylor
Phys. Rev. 75, 1352 (1949)

II. Lateral Spread of Particles in Cascade Showers

1. INTRODUCTION

The lateral structure of large air showers has been under extensive investigation. Euler and Wergeland[1] first calculated the expected distribution functions rather crudely. Moliere[2] later improved on their calculations and obtained the radial distribution of both electrons and photons as well as the angular distribution of electrons. These calculations do not take into account energy loss of electrons by ionization (approximation A of Rossi and Greisen[3]). Under the same approximation, Belenky[4] also calculated the angular distribution of electrons, but with better accuracy. Others, Roberg and Nordheim[5], e.g., have calculated quite accurately the mean square angles and displacements integrated over the shower for electrons and photons down to rather low energies, where ionization losses become important. More recently, Borsellino[6] has calculated mean square values as a function of depth.

The reason that more calculations of the distribution functions themselves have not been made is that it is extremely difficult to solve the diffusion equations when the terms involving the lateral spread are included. It turns out, however, that it is easy to calculate the moments of these functions quite accurately. When the calculations are made, it is found that the "exact" moments do not agree very well with those obtained

from Moliere's distribution functions. This is especially true for large arguments. Now, knowing the moments for a function, one should be able to reconstruct the function. Mathematically this is feasible if the moments can be expressed in analytic form and if the function satisfies certain conditions. Moreover, the function so derived is unique. Since, however, we can not obtain the moments in proper form for such a procedure, we have tried to reconstruct the function graphically. That this is possible and gives a unique solution can only be inferred from several test examples which will be presented in the next section. It appears that a monotonically decreasing "smooth" function can be reconstructed from a knowledge of its first few moments, covering the region of interest. Since the distribution functions physically satisfy the above conditions, it seems highly reasonable to expect a good approximation to the function over a useful range of values.

In this paper, then, we first show in Section 2 how to reconstruct a function from its moments. In Section 3, we calculate the moments in approximation A at the shower maximum and obtain an asymptotic expansion down to twice the critical energy, taking into account loss of energy by ionization. In Section 4, we show how the moments may be obtained for varying depth of the shower, in approximation A only. Finally in Section 5 we calculate the actual distribution function using the moments found in the previous sections.

The basic assumptions of our calculations are that the scattering angles are small and that the asymptotic expressions for radiation and pair production are valid. The calculations hold for any element for which, at the energy considered, these assumptions are valid.

2. RECONSTRUCTION OF A FUNCTION FROM A FINITE NUMBER OF ITS MOMENTS

In this section we shall present some evidence for the fact that knowledge of the first few moments of a 'reasonable' function essentially determines the function over a limited range. We shall consider functions which are 'smooth', decrease monotonically from 0 to ∞, and which may or may not be singular at the origin. For physical reasons these will be the characteristics of the actual distribution functions that we shall seek later.

Our confidence that a few moments determine the function rather well rests on several 'experiments' in which known functions were reconstructed from about four known moments. After trying various analytical schemes* for these test cases we found that the

---

* While this work was being carried out we received a copy of a paper by L. V. Spencer and U. Fano entitled "Penetration and Diffusion of X-rays: VII. Calculation of Space Distributions by Polynomial Expansion". One of the points of their paper seems to be the same as that of this section, viz., the first few moments of a reasonable function essentially determine the function over a limited range. Unfortunately, the neat method of polynomial expansions that they describe is not directly applicable to our problem, since our functions may be singular at the origin.

most convenient method for reconstructing the function was simply to graph an arbitrary function, calculate its moments numerically, alter the function as indicated by the discrepancies from the correct moments, recalculate the moments, make a second correction and in this way approach a function which would give the correct moments.

The results for three functions we attempted to fit are given below. We think these cases give fairly strong evidence that in general one can with considerable accuracy reconstruct functions of the type considered from their moments.

The first function attempted was $f(x) = \frac{e^{-x^{1.25}}}{x}$. In this case the only information used was that $f(x) \cong \frac{1 - x^{1.25}}{x}$ for small x, and the values of f_0, f_2, f_4, f_6; where we define the n'th moment f_n by:

$$f_n = \frac{\int_0^\infty x^{n+1} f(x)\, dx}{\int_0^\infty x f(x)\, dx} \qquad (1)$$

The values of the exact function and its moments, and the final fitted function and its moments are given in Table I.

We see that the agreement is excellent. The fitted function begins to diverge from the true one around $x = 7$. This is not surprising, since the integrand of f_6 has its maximum near $x = 3.5$, and the lower moments have the maximum of their integrands at smaller x. Therefore, not much information about the function for large values of x is contained in the four moments given.

The data on two other sample functions that were fitted is given in Tables II and III. For these examples <u>only</u> the values of the moments were known and <u>not</u> the behavior at the origin.

If one can draw any conclusions from these examples, it would appear that one is easily able to fit a function over most of its range to within a few percent, even when not much care is taken in fitting the highest moment. One cannot, however, determine the behavior at the origin with any certainty. This fact is particularly troublesome because one often wants to know the cosmic-ray distribution functions near the origin. In the last two examples the errors become greater than 10% for x of the order of 0.3 or 0.4 and increase rapidly for smaller x. The reason that the behavior at the origin is not determinable is as follows. The integrand for the n'th moment is of the form $x^{n+1} f(x)$, and for increasing n the maximum of this function moves farther and farther along the x-axis. Moreover, this integrand vanishes very strongly for small x, so the high moments are essentially independent of the behavior of the function at the origin. Thus, most of the information about the origin is contained in the

second moment, but the integrand of even this moment vanishes very strongly at the origin. For example, if $f(x)$ has a $\frac{1}{x}$ singularity the integrand behaves like x^2. Unfortunately we know only the even moments; knowledge of f_1 would help considerably in the fitting the function for small x.

3. MOMENTS OF THE DISTRIBUTION FUNCTIONS IN SHOWERS

(a) Approximation A

In this section we derive expressions for the moments of the angular and radial distribution functions in a large shower for energies much greater than the critical energy*. We shall consider the distribution functions which have been integrated over the length of the shower. These will also be the distribution functions at the shower maximum, since the $\frac{dE}{E^2}$ energy spectrum of particles at the maximum is the same as the energy spectrum integrated over the length. Also, it will be convenient to assume that the showers we consider are initiated by a single electron of energy E_0 but the results are really independent of this particular boundary condition so long as the initiating particles have energies much larger than the energy of the electrons or photons in which we are interested.

---

* The essential results of Section 3.a appear in an unpublished thesis by L. Eyges (Dissertation, Cornell University, 1948). These results were derived independently by Professor John Blatt and incorporated into some lecture notes. We are very grateful to Professor Blatt for allowing us to see copies of these notes. We have profited from several illuminating observations in them, as well as from suggestions for notation.

We specify the lateral position and direction of an electron or photon in the shower by the coordinates x and y in a plane perpendicular to the shower axis and angles θ_x and θ_y in two perpendicular planes whose intersection is parallel to the shower axis. We denote by $\pi(E, \theta_x, \theta_y, x, y)$ or, more briefly, $\pi(E, \vec{\theta}, \vec{r})$ the number of particles of energy E at the point (x, y) in $dx\,dy$ travelling at an angle (θ_x, θ_y) in $d\theta_x\,d\theta_y$ and by $\gamma(E, \theta_x, \theta_y, x, y)$ the analogous quantity for photons. Then the diffusion equations which describe the propagation and scattering in the shower are[7]:

$$\delta(E_0 - E)\,\delta(x)\,\delta(y)\,\delta(\theta_x)\,\delta(\theta_y) = L_1(\pi, \gamma) + \frac{E_s^2}{4E^2}\left(\frac{\partial^2\pi}{\partial\theta_x^2} + \frac{\partial^2\pi}{\partial\theta_y^2}\right) - \theta_x\frac{\partial\pi}{\partial x} - \theta_y\frac{\partial\pi}{\partial y}, \tag{2.a}$$

$$0 = L_2(\pi, \gamma) - \theta_x\frac{\partial\gamma}{\partial x} - \theta_y\frac{\partial\gamma}{\partial y}, \tag{2.b}$$

where $E_s = 21$ Mev and in the notation of Rossi and Greisen[3], the integral operators L_1 and L_2 are

$$L_1(\pi,\gamma) = 2\int_0^1 \gamma\left(\frac{E}{u}, \vec{\theta}, \vec{r}\right)\psi(u)\,\frac{du}{u}$$

$$-\int_0^1 \left[\pi(E, \vec{\theta}, \vec{r}) - \frac{1}{1-v}\pi\left(\frac{E}{1-v}, \vec{\theta}, \vec{r}\right)\right]\phi(v)\,dv$$

$$+\,\varepsilon\,\frac{\partial\pi}{\partial E}\,(E, \vec{\theta}, \vec{r}) \quad , \qquad (3.a)$$

$$L_2(\pi,\gamma) = \int_0^1 \pi\left(\frac{W}{v}, \vec{\theta}, \vec{r}\right)\phi(v)\,\frac{dv}{v} - \sigma\,\gamma\,(W, \vec{\theta}, \vec{r}). \qquad (3.b)$$

In this section we will set ε equal to zero. This is approximation A of Rossi and Greisen. Defining $\pi_{mn}(E)$ as

$$\pi_{mn}(E) \equiv \iiiint_{-\infty}^{+\infty} (E, \theta_x, \theta_y, x, y)(x^m\,\theta_x^n + y^m\theta_y^n)\,d\theta_x\,d\theta_y\,dx\,dy, \qquad (4)$$

we have

$$(x^m\,\theta_x^n + y^m\,\theta_y^n)\ \underset{\text{for electrons}}{\text{average}} = \frac{\pi_{mn}}{\pi_{00}} \equiv \left\langle \pi_{mn}(E) \right\rangle , \qquad (5)$$

where π_{00} is just <u>twice</u> the electron track length, i.e.,

$$\pi_{00} = 2 \cdot Z_{\pi}(E_0, E) = 2 \cdot \frac{0.437\, E_0}{E^2} \qquad (6)$$

$\langle \gamma_{mn}(W) \rangle$ is defined analogously. Now we get a recursion relation for π_{mn} and γ_{mn}. We multiply equations (2.a, b) by $(x^m \theta_x^n + y^m \theta_y^n)$ and integrate over x, y, θ_x, θ_y. The terms containing derivatives with respect to the spatial variables are then transformed in the following typical manner. Consider

$$\iiiint_{-\infty}^{+\infty} (x^m \theta_x^n + y^m \theta_y^n)\, \theta_x \frac{\partial \pi}{\partial x}\, d\theta_x\, d\theta_y\, dx\, dy$$

$$= \iiiint_{-\infty}^{+\infty} \theta_x^{n+1}\, d\theta_x\, d\theta_y\, dy \int_{-\infty}^{+\infty} x^m \frac{\partial \pi}{\partial x}\, dx$$

$$+ \iiiint_{-\infty}^{+\infty} y^m \theta_y^n \theta_x\, d\theta_x\, d\theta_y\, dy \int_{-\infty}^{+\infty} \frac{\partial \pi}{\partial x}\, dx \quad .$$

The last term in the above equation vanishes since there are no electrons at infinitely large radial distances from the axis. Under the further assumption that the distribution function vanishes strongly enough at infinity we can integrate the first term on the right hand side by parts, whereupon it becomes

$$- m \iiiint_{-\infty}^{+\infty} \theta_x^{n+1}\, x^{m-1}\, \pi(E, \theta_x, \theta_y, x, y)\, d\theta_x\, d\theta_y\, dx\, dy \; .$$

If we carry out a similar integration by parts on terms like

$$\iiiint_{-\infty}^{+\infty} \frac{\partial^2 \pi}{\partial \theta_x^{\,2}} \left(x^m \theta_x^n + y^m \theta_y^n\right) d\theta_x \, d\theta_y \, dx \, dy$$

and remember, e.g., that

$$\iiiint_{-\infty}^{+\infty} \left(\theta_x^{n+1} x^{m-1} + \theta_y^{n+1} y^{m-1}\right) \pi(E, \theta_x, \theta_y, x, y) d\theta_x d\theta_y \, dx \, dy$$

$$= \pi_{n+1,\, m-1}(E) \quad ,$$

we finally find that our equations become:

$$0 = L_1(\pi_{mn}(E), \gamma_{mn}(W)) + \frac{E_s^{\,2}}{4E^2} n(n-1)\pi_{m,\, n-2}(E)$$

$$+ m\pi_{m-1,\, n+1}(E) \quad , \tag{7.a}$$

$$0 = L_2\left(\pi_{mn}(E), \gamma_{mn}(W)\right) + m\gamma_{m-1,\, n+1}(W) \quad . \tag{7.b}$$

Equations (7.a, b) have solutions of the following form:

$$\pi_{mn}(E) = \frac{\alpha_{mn} E_s^{m+n}}{E^{m+n+2}} \quad , \tag{8.a}$$

$$\gamma_{mn}(W) = \frac{\beta_{mn} E_s^{m+n}}{W^{m+n+2}} \quad , \tag{8.b}$$

where α_{mn} and β_{mn} are independent of E and W. If we substitute from (8.a, b) into (7.a, b) we are led to the following equations, for $E \neq E_0$

$$0 = -A(m+n+1)\alpha_{mn} + B(m+n+1)\beta_{mn} + \frac{E_s^2}{4}\, n(n-1)\alpha_{m,\,n-2} + m\alpha_{m-1,\,n+1}\,, \tag{9.a}$$

$$0 = C(m+n+1)\alpha_{mn} - \sigma\beta_{mn} + m\beta_{m-1,\,n+1}\,. \tag{9.b}$$

The functions A, B, C, and σ that appear here are the same as those that appear in ordinary shower theory and are defined by Equation 2.17a of Rossi and Greisen's article.

Since π_{00} and γ_{00} are known, one can solve Eq. (9.a, b) by successively putting: $m = 0$, $n = 2$; $m = 1$, $n = 1$; $m = 2$, $n = 0$; $m = 4$, $n = 0$; $m = 3$, $n = 1, \ldots$. The quantities α_{mn} and β_{mn} are then successively determined in the manner indicated by the following scheme:

$$(\alpha_{00}, \beta_{00})$$

$$(\alpha_{02}, \beta_{02}) \rightarrow (\alpha_{11}, \beta_{11}) \rightarrow (\alpha_{20}, \beta_{20})$$

$$(\alpha_{04}, \beta_{04}) \rightarrow (\alpha_{13}, \beta_{13}) \rightarrow \cdots$$

We have calculated α_{mn} and β_{mn} for m, n up to $m + n = 10$, and then used (5) to find $\langle \pi_{mn} \rangle$ and $\langle \gamma_{mn} \rangle$ over the same range. Our results are given in Tables IV and V. The moments for which $m + n$ is odd vanish by symmetry.

The infinite sequence of moments, whose first terms are given in these tables, determines in principle the distribution functions we desire. We shall see in the next sections what can be deduced about the distribution functions from the <u>partial</u> sequence above.

First, we shall use these moments to check Moliere's and Belenky's calculations of the distribution functions. Moliere has derived expressions for the radial distribution functions, integrated over all angles, for both electrons and photons and the angular distribution function, integrated over all lateral displacements, for electrons[2]. Belenky has calculated the angular distribution of electrons[4]. To determine the accuracy of Moliere's and Belenky's results we have calculated $\langle r^n \rangle$ and $\langle \theta^n \rangle$* from their distributions and compared these moments with those derived from Tables IV and V using, e.g., for electrons

$$\langle \pi_{m0} \rangle = \langle x^m + y^m \rangle = 2 \langle x^m \rangle = 2 \langle r^m \rangle \langle \cos^m \phi \rangle , \tag{10.a}$$

$$\langle \pi_{0n} \rangle = \langle \theta_x^n + \theta_y^n \rangle = 2 \langle \theta_x^n \rangle = 2 \langle \theta^n \rangle \langle \cos^n \phi \rangle . \tag{10.b}$$

---

* $r^2 = x^2 + y^2$ and $\theta^2 = \theta_x^2 + \theta_y^2$.

The results are given in Table VI. It is seen that there are large discrepancies between the exact moments and those of Moliere.

(b) Asymptotic Expansions for the Moments

We will now consider the problem of finding the distribution functions for energies where collision loss of electrons is not negligible, i.e., when we retain the term $\varepsilon \frac{\partial \pi}{\partial E}$ in Eq. (3.a). First, consider the equations for the track lengths, neglecting scattering. We call the electron track length $Z_\pi(E_0, E)$ and the photon track length $Z_\gamma(E_0, W)$. They satisfy the following equations:

$$\delta(E_0 - E) = L_1(Z_\pi, Z_\gamma) \quad , \tag{11.a}$$

$$0 = L_2(Z_\pi, Z_\gamma) \quad . \tag{11.b}$$

The procedure for obtaining an asymptotic solution for these equations, valid down to energies a few times the critical energy is well known[3]. One assumes that Z_π and Z_γ have their high energy form, modified by a correction factor in the form of a series in $\frac{\varepsilon}{E}$ and $\frac{\varepsilon}{W}$, respectively, i.e.,

$$Z_\pi(E_0, E) = \frac{.437\, E_0}{E^2} \sum_{n=0}^{\infty} a_n \left(\frac{\varepsilon}{E}\right)^n \tag{12.a}$$

$$Z_\gamma(E_0, W) = \frac{.437\, E_0}{\sigma W^2} \sum_{n=0}^{\infty} b_n \left(\frac{\varepsilon}{W}\right)^n \tag{12.b}$$

If one substitutes these expressions into (3.a, b) one gets the following infinite set of equations

$$\frac{b_n\, B(n+1)}{\sigma} - a_n\, A(n+1) = (n+1)\, a_{n-1}^{\cdot} \quad , \quad n = 1, 2, \ldots \tag{13.a}$$

$$b_n = C(n+1)\, a_n \tag{13.b}$$

The functions $A(n)$, $B(n)$, $C(n)$ in these equations are the same as those appearing in equations (9.a, b). These equations can be solved. One obtains, setting $a_0 = 1$:

$$Z_\pi(E_0, E) = \frac{.437\, E_0}{E^2} \left(1 - 1.638 \frac{\varepsilon}{E} + 2.799 \frac{\varepsilon^2}{E^2} - 5.312 \frac{\varepsilon^3}{E^3} + 11.18 \frac{\varepsilon^4}{E^4} + \ldots\right) , \tag{14.a}$$

$$Z_\gamma(E_0, W) = \frac{.572\, E_0}{W^2} \left(1 - .771 \frac{\varepsilon}{W} + .866 \frac{\varepsilon^2}{W^2} - 1.231 \frac{\varepsilon^3}{W^3} + 2.078 \frac{\varepsilon^4}{W^4} + \ldots\right) . \tag{14.b}$$

It is possible to take somewhat different forms than (12.a, b) for Z_π and Z_γ. Following Rossi and Greisen, one can assume:

$$Z_{\pi}(E_0, E) = \frac{.437\, E_0}{E^2} \frac{1}{\left(1 + \alpha_1 \frac{\varepsilon}{E} + \alpha_2 \frac{\varepsilon^2}{E^2} + \dots\right)^2}, \tag{15.a}$$

$$Z_{\gamma}(E_0, W) = \frac{.572\, E_0}{W^2} \frac{1}{\left(1 + \beta_1 \frac{\varepsilon}{W} + \beta_2 \frac{\varepsilon^2}{W^2} + \dots\right)} \tag{15.b}$$

Using the binomial expansion, (15.a, b) can be brought into the form (12.a, b) and the relationship between a_n, b_n and α_n, β_n can be determined. Doing this, one gets the well known expressions of Rossi and Greisen.

$$Z_{\pi}(E_0, E) = \frac{.437\, E_0}{E^2} \frac{1}{\left[1 + .819\left(\frac{\varepsilon}{E}\right) - .394\left(\frac{\varepsilon}{E}\right)^2 + .591\left(\frac{\varepsilon}{E}\right)^3 + \dots\right]^2} \tag{16.a}$$

$$Z_{\gamma}(E_0, W) = \frac{.572\, E_0}{W^2} \frac{1}{\left[1 + .771\left(\frac{\varepsilon}{W}\right) - .272\left(\frac{\varepsilon}{W}\right)^2 + .354\left(\frac{\varepsilon}{W}\right)^3 + \dots\right]} \tag{16.b}$$

We would like to emphasize that this last form for the track length is arbitrary in that one could assume series expansions in $\frac{\varepsilon}{E}$ and $\frac{\varepsilon}{W}$, raised to <u>any</u> power, and determine

the coefficients in the same way as above. The essential behavior of the series is not changed by writing it in a form other than that of (14.a, b). Thus, both (14.a, b) and (16.a, b) seem to be valid down to $\frac{\varepsilon}{E} \approx 1/3$, and break down for higher values. It is true that for numerical computation one sometimes needs fewer terms in the series when it is in the form (16.a, b). The coefficients in (14.a, b) increase slowly and in any computation if one continues either of the series up to the point where the terms begin to increase they give the same answer.

Now let us turn to the problem of calculating the moments when energy loss is taken into account. One transforms Eqs. (2.a, b) by integration by parts and defines π_{mn} and γ_{mn} as before. Eqs. (3.a) and (3.b) still hold with the understanding that in the operator $L_1(\pi_{mn}, \gamma_{mn})$ one retains the term $\varepsilon \frac{\partial \pi_{mn}}{\partial E}$. One can get a formal solution of these equations by setting

$$\pi_{mn}(E) = \frac{\alpha_{mn} E_s^{m+n}}{E^{m+n+2}} \sum_{\ell=0}^{\infty} a_{mn}^{(\ell)} \left(\frac{\varepsilon}{E}\right)^{\ell}, \tag{17.a}$$

$$\gamma_{mn}(W) = \frac{\beta_{mn} E_s^{m+n}}{W^{m+n+2}} \sum_{\ell=0}^{\infty} b_{mn}^{(\ell)} \left(\frac{\varepsilon}{W}\right)^{\ell}. \tag{17.b}$$

Putting these expressions into Eqs. (7.a, b) and equating to zero various powers of $\frac{\varepsilon}{E}$ and $\frac{\varepsilon}{W}$ one gets the following set of equations, for $\ell = 0, 1, 2 \ldots$.

$$\alpha_{mn}\, a_{mn}^{(\ell)}\, A(m+n+\ell+1) - \beta_{mn}\, b_{mn}^{(\ell)}\, B(m+n+\ell+1)$$

$$+ (m+n+\ell+1)\alpha_{mn}\, a_{mn}^{(\ell-1)} = \frac{E_s^2}{4}\, n(n-1)\alpha_{m,\,n-2}\, a_{m,\,n-2}^{(\ell)}$$

$$+ m\alpha_{m-1,\,n+1}\, a_{m-1,\,n+1}^{(\ell)} , \tag{18.a}$$

$$\alpha_{mn}\, a_{mn}^{(\ell)}\, C(m+n+\ell+1) - \sigma\beta_{mn}\, b_{mn}^{(\ell)} + m\beta_{m-1,\,n+1}\, b_{m-1,\,n+1}^{(\ell)} = 0 \tag{18.b}$$

In these equations $a_{mn}^{(0)} = b_{mn}^{(0)} = 1$ and $a_{mn}^{(-1)} = 0$. For $\ell = 0$, Eqs. (18.a, b) are identical with Eqs. (9.a, b). Thus, the quantities α_{mn} and β_{mn} are known from the work in section 3a. The quantities $a_{mn}^{(\ell)}$ and $b_{mn}^{(\ell)}$ can then be determined successively in the following sequence

$$a_{02}^{(1)},\ b_{02}^{(1)};\quad a_{02}^{(2)},\ b_{02}^{(2)};\ \ldots\ a_{11}^{(1)},\ b_{11}^{(1)};\quad a_{11}^{(2)},\ b_{11}^{(2)};\ \ldots$$

$$a_{20}^{(1)},\ b_{20}^{(1)};\quad a_{20}^{(2)},\ b_{20}^{(2)};\ \ldots\ a_{04}^{(1)},\ b_{04}^{(1)};\quad a_{04}^{(2)},\ b_{04}^{(2)};\ \ldots\ .$$

As before, we are not directly interested in π_{mn} and γ_{mn} but in these quantities divided by π_{00} and γ_{00} respectively. If we then formally carry out this division using $\pi_{00} = 2\, Z_{\pi}$

and $\gamma_{00} = 2Z\gamma$ as given by Eqs. (14.a, b), we get expressions for π_{mn} and γ_{mn} in the form of the high energy expressions multiplied by a series in powers of $\frac{\varepsilon}{E}$ or $\frac{\varepsilon}{W}$. For convenience in computation we can convert these series to the form

$$\left\langle \pi_{mn}(E) \right\rangle = \frac{\left\langle \pi_{mn} \right\rangle_{\varepsilon = 0}}{\left[\sum_{\ell = 0}^{\infty} \alpha_{mn}^{(\ell)} \left(\frac{\varepsilon}{E} \right)^{\ell} \right]^{m+n}} ,$$

$$\left\langle \gamma_{mn}(W) \right\rangle = \frac{\left\langle \gamma_{mn}(W) \right\rangle_{\varepsilon = 0}}{\left[\sum_{\ell = 0}^{\infty} \beta_{mn}^{(\ell)} \left(\frac{\varepsilon}{W} \right)^{\ell} \right]^{m+n}} .$$

We will not present here our numerical results for all the quantities $\alpha_{mn}^{(\ell)}$ and $\beta_{mn}^{(\ell)}$, since they are of no great interest. The quantities of real interest are $\left\langle r^n (E) \right\rangle$ and $\left\langle \theta^n (W) \right\rangle$. In the Tables VII and VIII we present our results for these quantities.

It is hard to estimate the range of validity of the series in the denominators of the expressions in Tables VII and VIII. First, we have derived them purely formally, and in the process have divided dubiously convergent series into one another. Also, it is clear that for small $\frac{E}{\varepsilon}$ and $\frac{W}{\varepsilon}$ they diverge rather violently, particularly for the higher radial moments. Nevertheless, it is probably all right to use them, provided one terminates the series when the terms start to increase. The reason we believe this to be so is that the series for the track lengths in Eq. (14) seems to show the same dubious convergence, but they have been checked and found to be quite accurate for $\frac{E}{\varepsilon}$ greater then two or three. As a further check we have compared our results for the mean squares with the fairly accurate calculations of Roberg and Nordheim and find fairly good agreement. The comparison is given in Table IX.

The discrepancies between our values and those of Roberg and Nordheim for high energies are due to the fact that they did not use the usual asymptotic expression for the radiation cross section, but an approximation to it. The discrepancies at lower energies may also be partly due to this fact, but more probably arise because the Roberg-Nordheim calculation is much more accurate than ours. It is worth noting that our results for the moments of the angular distribution are valid down to somewhat lower energies than for the radial distribution. This is also true for the higher order moments; from Table VII and VIII we see that the series for the higher radial moments converges more poorly than that for the angular moments of the same order.

4. MOMENTS OF THE DISTRIBUTION FUNCTIONS AS A FUNCTION OF SHOWER DEPTH (APPROXIMATION A).

If we consider the variation of number of particles with the depth of the shower, equations (7.a, b) can be rewritten as

$$\frac{\partial \pi_{mn}(E,t)}{\partial t} = L_1\left(\pi_{mn}(E,t),\ \gamma_{mn}(W,t)\right) + \frac{E_s^2}{4E^2}\, n(n-1)\pi_{m,\,n-2}(E,t)$$

$$+\ m\pi_{m-1,\,n+1}(E,t) \quad , \tag{19.a}$$

$$\frac{\partial \gamma_{mn}(E,t)}{\partial t} = L_2\left(\pi_{mn}(E,t),\ \gamma_{mn}(W,t)\right) + m\,\gamma_{m-1,\,n+1}(W,t) \ . \tag{19.b}$$

These can be solved by performing a Mellin and Laplace transform and doing the final integration by the saddle point method, just as in the case of the longitudinal shower. This means introducing

$$N(\pi_{mn};\ s,\lambda) \equiv \int_0^\infty dt \int_0^\infty dE\ e^{-\lambda t}\ E^s \pi_{mn}(E_o,\ E,\ t) \tag{20.a}$$

and

$$N(\gamma_{mn};\ s,\lambda) \equiv \int_0^\infty dt \int_0^\infty dE\ e^{-\lambda t}\ E^s \gamma_{mn}(E_o,\ E,\ t) \quad , \tag{20.b}$$

then solving for the N's.

$$N(\pi_{mn};\, s,\lambda) = \frac{n(n-1)}{4}\, E_s^2\, \frac{(\lambda+\sigma)\, N(\pi_{m,\, n-2};\, s-2,\lambda)}{[\lambda-\lambda_1(s)][\lambda-\lambda_2(s)]}$$

$$+ \frac{m\, (\lambda+\sigma)\, N(\pi_{m-1,\, n+1};\, s,\lambda)}{[\lambda-\lambda_1(s)][\lambda-\lambda_2(s)]}$$

$$+ \frac{m B(s)\, N(\gamma_{m-1,\, n+1};\, s,\lambda)}{[\lambda-\lambda_1(s)][\lambda-\lambda_2(s)]}\,, \tag{21.a}$$

$$N(\gamma_{mn};\, s,\lambda) = \frac{n(n-1)}{4}\, E_s^2\, \frac{C(s)\, N(\pi_{m,\, n-2};\, s-2,\lambda)}{[\lambda-\lambda_1(s)][\lambda-\lambda_2(s)]}$$

$$+ \frac{m\, C(s)\, N(\pi_{m-1,\, n+1};\, s,\lambda)}{[\lambda-\lambda_1(s)][\lambda-\lambda_2(s)]}$$

$$+ \frac{m(\lambda+A(s))\, N(\gamma_{m-1,\, n+1};\, s,\lambda)}{[\lambda-\lambda_1(s)][\lambda-\lambda_2(s)]} \tag{21.b}$$

where, as before $A(s)$, $B(s)$, $C(s)$, and σ are the functions which arise in longitudinal shower theory; and $\lambda_1(s)$ and $\lambda_2(s)$ are roots of the equation $[\lambda+A(s)][\lambda+\sigma] - B(s)\, C(s) = 0$.

All these functions are tabulated in Rossi and Greisen's review article.

The N's may now be calculated in sequence as in Section 3, namely, $m = 0$, $n = 2$; $m = 1$, $n = 1$; $m = 2$, $n = 0$; $m = 0$, $n = 4$; $n = 1$, $n = 3$; ... . It is then easy to invert the Laplace transform for each case of the sequence after substituting for the N's of lower order. The simplest case is that for $N(\pi_{02}; s, \lambda)$. In this expression $N(\pi_{00}, s - 2, \lambda)$ must be replaced by <u>twice</u> the value given by Rossi and Greisen, i.e.,

$$\frac{2(\lambda + \sigma)\, E_o^{\,s-2}}{\left[\lambda - \lambda_1(s-2)\right]\left[\lambda - \lambda_2(s-2)\right]}$$

where E_o is the energy of the initiating electron.

The result of the inversion is :

$$M(\pi_{02}; s, t) = \left(\frac{E_s}{E_o}\right)^2 E_o^s \cdot$$

$$\left\{ \frac{\left[\lambda_1(s) + \sigma\right]^2 \exp\left[\lambda_1(s)\, t\right]}{\left[\lambda_1(s) - \lambda_2(s)\right]\left[\lambda_1(s) - \lambda_1(s-2)\right]\left[\lambda_1(s) - \lambda_2(s-2)\right]} \right.$$

$$+ \frac{\left[\lambda_2(s) + \sigma\right]^2 \exp\left[\lambda_2(s) t\right]}{\left[\lambda_2(s) - \lambda_1(s)\right]\left[\lambda_2(s) - \lambda_1(s-2)\right]\left[\lambda_2(s) - \lambda_2(s-2)\right]}$$

$$+ \frac{\left[\lambda_1(s-2) + \sigma\right]^2 \exp\left[\lambda_1(s-2)\, t\right]}{\left[\lambda_1(s-2) - \lambda_1(s)\right]\left[\lambda_1(s-2) - \lambda_2(s)\right]\left[\lambda_1(s-2) - \lambda_2(s-2)\right]}$$

$$\left. + \frac{\left[\lambda_1(s-2) + \sigma\right]^2 \exp\left[\lambda_2(s-2)\, t\right]}{\left[\lambda_2(s-2) - \lambda_1(s)\right]\left[\lambda_2(s-2) - \lambda_2(s)\right]\left[\lambda_2(s-2) - \lambda_1(s-2)\right]} \right\}.$$

π_{02} can be determined by a saddle point integration of each of the above terms just as in the case of the longitudinal shower theory. In the above expression $\left[\lambda_2(s) - \lambda_2(s-2)\right]$ has a zero at $s \cong 2.7$, so one has to be careful in the evaluation. It turns out that*

$$\pi_{02}(E_o, E, t) = \frac{1}{(2\pi)^{\frac{1}{2}}} \left(\frac{E_s}{E}\right)^2 \cdot \tag{23}$$

$$\frac{1}{E}\left\{\frac{\left[\lambda_1(s_1)+\sigma\right]^2\left(\frac{E_o}{E}\right)^{s_1-2}\left[\lambda_1''(s_1)\,t\right]^{-\frac{1}{2}}\exp\left[\lambda_1(s_1)\,t\right]}{\left[\lambda_1(s_1)-\lambda_2(s_1)\right]\left[\lambda_1(s_1)-\lambda_1(s_1-2)\right]\left[\lambda_1(s_1)-\lambda_2(s_1-2)\right]}\right.$$

$$+\frac{\left[\lambda_2(s_2)+\sigma\right]^2\left(\frac{E_o}{E}\right)^{s_2-2}\left[\lambda_2''(s_2)t+(s_2-s_o)^{-2}\right]^{-\frac{1}{2}}\exp\left[\lambda_2(s_2)\,t\right]}{\left[\lambda_2(s_2)-\lambda_1(s_2)\right]\left[\lambda_2(s_2)-\lambda_1(s_2-2)\right]\left[\lambda_2(s_2)-\lambda_2(s_2-2)\right]}$$

$$+\frac{\left[\lambda_1(s_1)+\sigma\right]^2\left(\frac{E_o}{E}\right)^{s_1}\left[\lambda_1''(s_2)\,t\right]^{-\frac{1}{2}}\exp\left[\lambda_1(s_1)\,t\right]}{\left[\lambda_1(s_1)-\lambda_1(s_1+2)\right]\left[\lambda_1(s_1)-\lambda_2(s_1+2)\right]\left[\lambda_1(s_1)-\lambda_2(s_1)\right]}$$

$$\left.+\frac{\left[\lambda_2(s_2)+\sigma\right]^2\left(\frac{E_o}{E}\right)^{s_2}\left[\lambda_2''(s_2)\,t+(s_2-s_o)^{-2}\right]^{-\frac{1}{2}}\exp\left[\lambda_2(s_2)\,t\right]}{\left[\lambda_2(s_2)-\lambda_2(s_2+2)\right]\left[\lambda_2(s_2)-\lambda_2(s_2+2)\right]\left[\lambda_2(s_2)-\lambda_1(s_2)\right]}\right\}.$$

---

* These expressions for the second moment appear in the notes of Professor Blatt, mentioned previously.

where s_o, s_1, and s_2 are defined by

$$\lambda_2(s_o) = \lambda_2(s_o - 2)$$

$$\lambda_1'(s_1)\, t + \log \frac{E_o}{E} = 0$$

$$\lambda_2'(s_2)\, t + \log \frac{E_o}{E} - (s_2 - s_o)^{-1} = 0 \quad .$$

In equation (23) it is apparent that the first two terms are small compared with the last two respectively, especially for large values of $\frac{E_o}{E}$ since the terms are in the ratio of $\left(\frac{E_o}{E}\right)^{-2}$. Also for reasonable values of t, $\lambda_2(s_2)$ is sufficiently more negative than $\lambda_1(s_1)$ to make the fourth term small compared to the third term. If then, t is not too small, we can write, dropping the subscript on s.

$$\pi_{02}(E_o, E, t) \cong \frac{1}{(2\pi)^{\frac{1}{2}}} \left(\frac{E_s}{E}\right)^2 \cdot \tag{24}$$

$$\frac{1}{E} \frac{\left[\lambda_1(s) + \sigma\right]^2 \left(\frac{E_o}{E}\right)^s \left[\lambda_1''(s)\, t\right]^{-\frac{1}{2}} \exp\left[\lambda_1(s)\, t\right]}{\left[\lambda_1(s) - \lambda_1(s+2)\right]\left[\lambda_1(s) - \lambda_2(s+2)\right]\left[\lambda_1(s) - \lambda_2(s)\right]} \cdot$$

For each pair of values of m and n we find a similar situation, that is, we find that $\pi_{mn}(E_o, E, t)$ can be approximated by one term of the many involved in the double

transform. Succeeding terms of the sequence become so involved that we shall not write them here. The procedure, however, is exactly as in the case above.

From these expressions, we obtain the moments by dividing by

$$\pi_{00}(E_o, E, t) = \frac{1}{(2\pi)^{\frac{1}{2}}} \left(\frac{E_o}{E}\right)^s \cdot \tag{25}$$

$$\frac{1}{E} \frac{\left[\sigma + \lambda_1(s)\right] \left[\lambda_1''(s)\, t\right]^{-\frac{1}{2}} \exp\left[\lambda_1(s)\, t\right]}{\left[\lambda_1(s) - \lambda_2(s)\right]} .$$

In this manner, we have calculated the angular moments for both electrons and photons as well as the radial moments for electrons as a function of parameter s. The relationship between s and the depth of the shower is given through the usual expression, $\log (E_o/E) + \lambda_1'(s)\, t = 0$. Figs. 1, 2, and 3 show the variation of the angular electron and photon moments and radial electron moments, respectively with s. An analytic expression for the angular moments is easily obtained. In terms of the functions used above, these are

$$\left(\frac{E}{E_s}\right)^n \left\langle \theta^n \right\rangle_{\text{electrons}} = \frac{n!}{2^{n-1}} \left[\lambda_1(s) + \sigma\right]^{n/2} \cdot \tag{26.a}$$

$$\prod_{k=1}^{n/2} \frac{1}{\left[\lambda_1(s) - \lambda_1(s+n)\right]\left[\lambda_1(s) - \lambda_2(s+n)\right]} ,$$

$$\left(\frac{W}{E_s}\right)^n \left\langle \theta^n \right\rangle_{\text{photons}} = \frac{C(s+n)}{C(s)} \left(\frac{E}{E_s}\right)^n \left\langle \theta^n \right\rangle_{\text{electrons}} . \tag{26.b}$$

Similar expressions have been obtained by Borsellino[6]. The radial moments cannot be written in such simple form and will not be given here.

5. THE DISTRIBUTION FUNCTIONS

(a) Approximation A

We now turn to the problem of calculating the actual distribution function under approximation A, using the moments found in Sections 3a and 4. We will concern ourselves with the angular distribution integrated over all displacements; from symmetry these distributions are a function of $\theta = (\theta_x^2 + \theta_y^2)^{\frac{1}{2}}$. Similarly, the radial distributions are a function only of $r = (x^2 + y^2)^{\frac{1}{2}}$. Moreover, from the structure of the equations, the distributions depend on E, r and W, r through the combination Er/E_s and Wr/E_s. We can denote both of these quantities by x without confusion. The angular distributions depend on $\frac{E\theta}{E_s}$ and $\frac{W\theta}{E_s}$, both of which we call y. r is measured in radiation units and θ in radians. We shall call

$P_r\left(\frac{Er}{E_s}\right) \equiv P_r(x)$ the radial distribution of electrons and

$P_\theta\left(\frac{E\theta}{E_s}\right) \equiv P_\theta(y)$ the angular distribution of electrons.

Similarly we call $Q_r(\frac{Wr}{E_s}) \equiv Q_r(x)$ the radial distribution of quanta and $Q_\theta(\frac{W\theta}{E_s})$ the angular distribution. The distribution functions are defined so that $P_r(\frac{Er}{E_s})r\,dr$ is proportional to the number of electrons of energy E in the annular ring between r and $r + dr$, and $P_\theta(\frac{E\theta}{E_s})\theta\,d\theta$ is proportional to the number of electrons of energy E in the solid angle between θ and $\theta + d\theta$. We normalize the functions so that $\int_0^\infty P_r(x)x\,dx = 1$ and $\int_0^\infty P_\theta(y)y\,dy = 1$ and similarly for the photons.

Consider first the radial distribution of electrons at the shower maximum ($s = 1$). As we have explained in Section 2, our method of fitting functions by their moments does not give the behavior near the origin. For the higher moments Moliere's function seems to be quite inaccurate, but the second moment, which depends most sensitively on the behavior near the origin differs from the correct value by only 12%. It seems reasonable then to assume that Moliere's function is essentially correct for small x, and to start calculations on this basis. Actually, we reversed the procedure and used the higher moments first, i.e., we found the form of the function for large x and worked down toward the origin. If one can base an estimate on the examples in Section 2, our function should be quite accurate down to about an x of 0.4. Our function joins smoothly to Moliere's at this point. In Table X, column 2 we present our results.

In calculating the radial distribution of photons there is again the difficulty that the distribution function has a singularity at the origin. For this case also, the second moment as calculated from Moliere's distribution function is not very different from the exact moment. We have felt justified then in assuming his distribution function to be correct up to $x = 0.4$, and calculating the function for higher values from the moments. The results are given in Table X, column 3.

The calculation of the angular distribution of electrons is somewhat simpler than for the above two cases, since there is no singularity at the origin. Our results are given in Table X, column 4.

The angular distribution of photons can of course be calculated by the same methods we have used for the other distributions. Alternately, it is clear on physical grounds that it is determined once the angular distribution of electrons is known, since photons are not scattered, but inherit their angular distribution from parent electrons of higher energy. Mathematically, this is clear from Eqs. (2.b) and (3.b) which give

$$Q_\theta \left(\frac{E\theta}{E_s} \right) = \frac{1}{\sigma} \int_0^1 P_\theta \left(\frac{E\theta}{E_s v} \right) \phi(v) \frac{dv}{v} \quad .$$

If we take $\phi(v) = 1/v$ and write $y = \frac{E\theta}{E_s}$

$$Q_\theta(y) = \frac{1}{\sigma} \int_0^1 P_\theta \left(\frac{y}{v} \right) \frac{dv}{v^2} \quad .$$

Now to a rough approximation $P_\theta(y)$ is just an exponential,

$$P_\theta(y) \approx 12 \exp \left(-\sqrt{12}\, y \right) \quad .$$

Therefore,

$$Q_\theta(y) \approx \frac{12}{\sigma} \int_0^1 \exp \left(-\sqrt{12}\, \frac{y}{v} \right) \frac{dv}{v^2} \propto \frac{\exp \left(-\sqrt{12}\, y \right)}{y}$$

is an approximation to the angular distribution of photons. We have improved on this approximation by the method of moments, assuming that the above expression for $Q_\theta(y)$ is almost correct near the origin. Our results are given in the last column of Table X.

It is interesting to compare the results of our calculations of the distribution functions with those of Moliere. Figures 4 - 6, curves A and M show the results of the high energy approximation at shower maximum as derived from the moments and as calculated by Moliere, respectively. Consider first $P_\theta(y)$ in Figure 4. Our calculations agree with Moliere's to within a few percent up to $y = 1.7$. Beyond this point Moliere's function becomes smaller than ours by a factor 0.91 at $y = 2$ and 0.36 at $y = 2.5$. Near $y = 3$, Moliere's function becomes negative. Our calculations

of $Q_r(x)$, Figure 5, also agree with Moliere's to within a few percent up to $x = 0.5$. At this point they begin to differ, but by no more than 25% even up to $x = 5$. The greatest difference between our calculations and Moliere's is in $P_r(x)$, shown in Figure 6. There is good agreement up to approximately $x = 0.6$. At this point Moliere's function begins to drop below ours and becomes lower by a factor 0.85 at $x = 1.2$. Moliere's curve then crosses ours at $x = 1.8$ and exceeds it by a factor of 2 at $x = 3.5$. It then again approaches ours and crosses in the opposite direction at $x = 5.5$.

(b) Effect of Collision Loss

We now turn to the problem of calculating the distribution function for energies when collision loss is not negligible, using the moments derived in Section 3a for $s = 1$. There are no essential differences in this work from that of Section 5a; the main difficulty here is that for the lowest energies with which we deal the behavior of our series for the moments is rather dubious. For energies down to about five times the critical energy the latter difficulty is probably not very serious; our expressions for the moments are probably accurate within a few percent. Moreover, we are helped by the following fact: as one goes down in energy the distribution functions become steeper and their shape over the range of interest becomes less sensitive to the less accurate higher moments.

Also, when collision loss is included we have less knowledge of the behavior of the functions at the origin. In Approximation A, for $s = 1$ we could rely more or less on Moliere's calculations; in the present case we must guess. The best guess seems to be that the singularities at the origin are the same as for high energies. Thus, from Table VII we see that the effect of collision loss on the moments is least for the lower order moments, i.e., for small distances and angles. It does not seem unreasonable then to guess that the behavior of the distribution functions for small values of their arguments is unchanged from that when collision loss is neglected. In calculating the distribution functions, however, we have not made use of this guess. The functions away from the origin are determined by the moments and we have calculated them in the same way as the examples in Section 2. Thus it seems that the functions are determined fairly accurately down to x or y of about 0.4. Nevertheless, we present our values down to 0.2 in Tables XI and XII for $E = 10\mathcal{E}$ and $E = 5\mathcal{E}$, respectively.

We have also calculated the distribution functions for $E = 2\mathcal{E}$. For this case, the expressions for the radial moments are probably very inaccurate, and our radial distributions may very well be quite far off. The numbers in Table XIII thus represent an educated guess rather than a reliable calculation. The angular distribution functions are probably somewhat more accurate than the radial functions since the expressions for the

angular moments converge much better than those for the radial moments. But even so one cannot put much faith in even the angular functions since the asymptotic cross sections we have used are poor approximations at this energy even for the ligher elements.

The distribution functions for the cases $E = 10\mathcal{E}$, $5\mathcal{E}$, and $2\mathcal{E}$ are also plotted in Figures 4 - 6, being marked B, C, and D, respectively. It is seen that the lower the energy, the steeper the function and the fewer the particles at large distances from the shower core.

(c) Distribution Functions at other Shower Depths

We have also calculated the distribution functions for $s = 0.6$ and 1.5. These correspond approximately to a depth equal to half the shower maximum and twice the shower maximum, respectively. Again, our method of reconstructing the function from a finite number of moments does not give us the behavior near the origin very accurately, especially if there happens to be a singularity at the origin. $P_\theta(x, s)$ is not singular and should be quite accurate down to $x \approx 0.3$, $Q_\theta(y, s)$ is singular and goes like $1/y$ for small y and $s = 1$. For $s = 0.6$ and 1.5, a $1/y$ singularity is consistent with our results also, although it seems clear that for $s = 0.6$ the singularity should be stronger than for $s = 1.5$. Mainly for ease in expressing the normalization, we have assumed that the singularity is exactly $1/y$ for both $s = 0.6$ and $s = 1.5$.

In Tables XIV and XV we present the results for the high energy angular distribution functions for $s = 0.6$, 1, and 1.5. These are also shown graphically in Figures 7 and 8.

The radial distribution of electrons is also singular at the origin, this singularity being of order $r^{-1/3}$ at the shower maximum, if we assume Moliere's calculation to give an accurate picture of the shower spread for small r. In calculating the distribution functions for $s = 0.6$ and 1.5, we again assume the functions singular, but have no way of specifying the order of the singularity. This means that we have to guess the behavior of the function for small r. Since the major contribution to the area under the distribution function, namely $\langle r^0 \rangle$ comes from small r, the amplitude of the function is not greatly changed at large r so long as we continue the curve back toward the origin smoothly and make $\langle r^0 \rangle$ unity. The shape of the function for large r is correct, since it depends only on the higher moments and not at all on the type of singularity. The amplitude, however, does depend to a slight extent on how well we have guessed the behavior at the origin. The normalization, therefore, may be off by several percent. In Table XVI we present our results for $x > 0.2$, but we do not believe the value for $x = 0.2$ to be very reliable. Figure 9 shows the results graphically.

REFERENCES

1. H. Euler and H. Wergeland, Astrophysica Norvegica 3, 165 (1940).
2. G. Moliere, Cosmic Radiation, ed. Heisenberg (Dover, 1946); Z. Phys. 125, 250 (1948); Phys. Rev. 77, 715 (1950).
3. B. Rossi and K. Greisen, Rev. Mod. Phys. 13, 240 (1941).
4. S. Belenky, J. Phys. U. S. S. R. 8, 9 (1944).
5. J. Roberg and L. Nordheim, Phys. Rev. 75, 444 (1949).
6. A. Borsellino, Nuovo Cimento 6, 543 (1949); 7, 638 (1950).
7. L. Landau, J. Phys. U. S. S. R. 3, 237 (1940).

Table I

Reconstruction of $\frac{e^{-x^{1.25}}}{x}$ from Four Moments

and the Knowledge of Its Behavior at the Origin.

n	f_n(exact)	f_n(fitted)	x	$xf(x) = e^{-x^{1.25}}$	xf(x)(fitted)
0	1	1	0	1.00	1.00
2	1.066	1.069	.5	.656	.661
4	5.15	5.16	1.0	.368	.358
6	52.8	53.5	2.0	.0928	.0930
			3.0	.0193	.0187
			4.0	.00339	.00339
			5.0	.00058	.00056
			6.0	.000087	.000087
			7.0	.000012	.000020

Table II

Reconstruction of $i\,H_0^{(1)}(ix)$ from Four Moments*.

n	f_n(exact)	f_n(fitted)	x	$f(x) = i\,H_0^{(1)}(ix)$	f(x)(fitted)
0	1.00	1.00	.1	4.85	2.98
2	4.00	4.11	.2	3.51	2.59
4	64.0	65.4	.3	2.74	2.25
6	2304	2212	.4	2.23	1.96
			.6	1.56	1.45
			.8	1.13	1.11
			1.0	.842	.843
			2.0	.228	.228
			3.0	.0695	.0674
			4.0	.0223	.0226
			5.0	.00738	.00732
			6.0	.00249	.00259
			7.0	.000849	.000846

---

* The Hankel function $iH_0^{(1)}(ix)$ is defined as in Jahnke-Emde, Tables of Functions, Dover (1945).

Table III

Reconstruction of $f(x) = \frac{e^{-x}}{x}$ from Four Moments.

n	f_n(exact)	f_n(fitted)	x	$f(x) = \frac{e^{-x}}{x}$	f(x)(fitted)
0	1.00	1.00	.1	2.86	1.90
2	3.75	3.67	.2	1.83	1.53
4	59.1	58.4	.3	1.35	1.24
6	2112.	2382.	.4	1.06	1.03
			.6	.708	.725
			.8	.502	.519
			1.0	.368	.390
			2.0	9.55×10^{-2}	.100
			3.0	2.87	2.75×10^{-2}
			4.0	9.15×10^{-3}	8.34×10^{-3}
			5.0	3.03	2.78
			6.0	1.01	9.36×10^{-4}
			7.0	3.44×10^{-4}	3.30
			8.0	1.18	1.20
			10.0	1.44×10^{-5}	1.75×10^{-5}
			12.0	1.77×10^{-6}	2.81×10^{-6}

TABLE IV

Evaluation of $\left\langle \pi_{mn}(E) \right\rangle = \dfrac{\iiiint_{-\infty}^{+\infty} \pi(E, \theta_x, \theta_y, x, y)(x^m \theta_x^n + y^m \theta_y^n) d\theta_x \, d\theta_y \, dx \, dy}{\iiiint_{-\infty}^{+\infty} \pi(E, \theta_x, \theta_y, x, y) \, d\theta_x \, d\theta_y \, dx \, dy}$

in Approximation A. The tabulated quantities are $\left(\frac{E}{E_s}\right)^{m+n} \cdot \pi_{mn}(E)$.

m \ n	0	1	2	3	4	5	6	7	8	9	10
0	2.00	0	.570	0	.719	0	1.94	0	8.81	0	59.5
1	0	.394	0	.579	0	1.77	0	8.98	0	66.8	
2	.725	0	.754	0	2.24	0	11.7	0	91.1		
3	0	1.48	0	3.93	0	19.7	0	131			
4	5.43	0	10.6	.0	47.0	0	315				
5	0	45.7	0	1.72×10^2	0	1.07×10^3					
6	3.10×10^2	0	$.970 \times 10^3$	0	5.48×10^3						
7	0	7.56×10^3	0	3.94×10^4							
8	7.57×10^4	0	3.62×10^5								
9	0	3.97×10^6									
10	5.09×10^7										

TABLE V

Evaluation of $$\left\langle \gamma_{mn}(W) \right\rangle \equiv \frac{\iiiint_{-\infty}^{+\infty} \gamma(W, \theta_x, \theta_y, x, y)(x^m \theta_x^n + y^m \theta_y^n)\, d\theta_x\, d\theta_y\, dx\, dy}{\iiiint_{-\infty}^{+\infty} \gamma(W, \theta_x, \theta_y, x, y)\, d\theta_x\, d\theta_y\, dx\, dy}$$

in Approximation A. The tabulated quantities are $\left(\frac{W}{E_s}\right)^{m+n} \cdot \gamma_{mn}(W)$.

m \ n	0	1	2	3	4	5	6	7	8	9	10
0	2.00	0	.176	0	.134	0	.259	0	.922	0	5.12
1	0	.350	0	.280	0	.573	0	2.13	0	12.4	
2	1.13	0	.864	0	1.78	0	6.74	0	38.9		
3	0	3.63	0	7.43	0	28.2	0	166			
4	19.8	0	39.8	0	1.51×10^2	0	885				
5	0	2.64×10^2	0	$.992 \times 10^3$	0	5.81×10^3					
6	2.085×10^3	0	7.79×10^3	0	4.55×10^4						
7	0	7.13×10^4	0	4.15×10^5							
8	7.45×10^5	0	4.32×10^6								
9	0	5.06×10^7									
10	6.59×10^8										

TABLE VI

Comparison of Exact Moments with Those Derived from the Distribution Functions Calculated by Moliere and Belenky.

	Electrons: $\langle r^n \rangle_{Av} \cdot \left(\frac{E}{E_s}\right)^n$		Photons: $\langle r^n \rangle_{Av} \left(\frac{W}{E_s}\right)^n$	
n	Moliere	Exact*	Moliere	Exact
0	1	1	1	1
2	0.830	0.725	1.02	1.13
4	6.40	7.24	16.0	26.4
6	1.06×10^2	4.95×10^2	5.45×10^2	3.34×10^3
8	2.76×10^3	1.38×10^5	3.19×10^4	1.36×10^6
10	1.03×10^5	1.03×10^8	2.85×10^6	1.34×10^9

	Electrons: $\langle \theta^n \rangle_{Av} \cdot \left(\frac{E}{E_s}\right)^n$			Photons: $\langle \theta^n \rangle_{Av} \cdot \left(\frac{W}{E_s}\right)^n$
n	Moliere	Belenky	Exact	Exact
0	1	1	1	1
2	0.602	0.655	0.570	0.176
4	1.72	1.43	0.959	0.178
6	30.4	6.56	3.10	0.415
8	1.12×10^3	51.6	16.1	1.69
10	5.42×10^4	620	121	10.4

* Similar results for the exact radial moments of electrons have been obtained by L. W. Nordheim, L. Osborne and J. Blatt, Proceedings of the Echo Lake Cosmic Ray Symposium, December, 1949.

TABLE VII

Electron Moments Including Correction for Ionization Loss.

$$\left\langle r^m \right\rangle_\varepsilon = \left\langle r^m \right\rangle_{\varepsilon = 0} \Bigg/ \left[1 + \sum_{\ell = 1}^{\infty} \alpha_{m0}^{(\ell)} \left(\frac{\varepsilon}{E} \right)^{\ell} \right]^m$$

$\alpha_{m0}^{(\ell)}$

ℓ \ m	2	4	6
1	1.73	1.60	1.52
2	-1.16	-2.02	-2.53
3	2.57	5.42	6.62
4	-7.60	-19.6	-30.8

$$\left\langle \theta^n \right\rangle_\varepsilon = \left\langle \theta^n \right\rangle_{\varepsilon = 0} \Bigg/ \left[1 + \sum_{\ell = 1}^{\infty} \alpha_{0n}^{(\ell)} \left(\frac{\varepsilon}{E} \right)^{\ell} \right]^n$$

$\alpha_{0n}^{(\ell)}$

ℓ \ n	2	4	6
1	.813	.915	1.02
2	-.747	-.950	-1.17
3	1.46	2.09	2.88
4	-3.73	-6.05	-9.31

TABLE VIII

Photon Moments Including Correction for Ionization Loss.

$$\langle r^m \rangle_\varepsilon = \langle r^m \rangle_{\varepsilon=0} \Big/ \left[1 + \sum_{\ell=1}^{\infty} \beta_{m0}^{(\ell)} \left(\frac{\varepsilon}{W}\right)^{\ell} \right]^m$$

$\beta_{m0}^{(\ell)}$

ℓ \ m	2	4	6
1	1.32	1.16	1.21
2	- .766	-1.10	-1.95
3	1.54	2.52	2.66
4	-3.80	-7.71	-13.0

$$\langle \theta^n \rangle_\varepsilon = \langle \theta^n \rangle_{\varepsilon=0} \Big/ \left[1 + \sum_{\ell=1}^{\infty} \beta_{0n}^{(\ell)} \left(\frac{\varepsilon}{W}\right)^{\ell} \right]^n$$

$\beta_{0n}^{(\ell)}$

ℓ \ n	2	4	6
1	.836	.916	1.01
2	- .556	- .755	- .952
3	.949	1.50	2.23
4	-2.15	-3.98	-6.70

TABLE IX

Comparison of Mean Squares with Calculations of Roberg-Nordheim.

Electrons

$\frac{E}{\mathcal{E}}$	$\left(\frac{E}{E_s}\right)^2 \cdot \langle \theta^2 \rangle$ Roberg-Nordheim	$\left(\frac{E}{E_s}\right)^2 \cdot \langle \theta^2 \rangle$ Present Calculations	$\left(\frac{E}{E_s}\right)^2 \cdot \langle r^2 \rangle$ Roberg-Nordheim	$\left(\frac{E}{E_s}\right)^2 \cdot \langle r^2 \rangle$ Present Calculations
∞	.545	.570	.642	.725
10	.47	.493	.49	.535
7	.44	.467	.46	.481
5	.42	.44	.43	.42
3	.38	.40	.40	.35
2	.34	.29	.33	.29

Photons

$\frac{W}{\mathcal{E}}$	$\left(\frac{W}{E_s}\right)^2 \cdot \langle \theta^2 \rangle$ Roberg-Nordheim	$\left(\frac{W}{E_s}\right)^2 \cdot \langle \theta^2 \rangle$ Present Calculations	$\left(\frac{W}{E_s}\right)^2 \cdot \langle r^2 \rangle$ Roberg-Nordheim	$\left(\frac{W}{E_s}\right)^2 \cdot \langle r^2 \rangle$ Present Calculations
∞	.181	.176	1.13	1.13
10	.16	.152	.95	.893
7	.15	.143	.88	.816
5	.14	.133	.80	.73
3	.12	.12	.71	.61
2	.11	.09	.62	.52

TABLE X

Distribution Functions in Approximation A.

	$x = \frac{Er}{E_s}$ or $\frac{Wr}{E_s}$		$y = \frac{E\theta}{E_s}$ or $\frac{W\theta}{E_s}$	
x or y	$P_r(x)$	$Q_r(x)$	$P_\theta(y)$	$Q_\theta(y)$
0	*	**	9.27	***
.1			7.13	
.2	7.62	7.33	5.35	8.60
.4	2.74	1.12	2.78	2.19
.6	1.01	3.73×10^{-1}	1.52	7.68×10^{-1}
.8	4.84×10^{-1}	1.96	8.20×10^{-1}	2.86
1.0	2.52	1.21	4.46	1.18
1.2	1.47	8.58×10^{-2}	2.32	4.56×10^{-2}
1.4	8.72×10^{-2}	6.04	1.18	1.96
1.6	5.36	4.55	6.04×10^{-2}	8.6×10^{-3}
1.8	3.49	3.48	2.90	3.82
2.0	2.26	2.67	1.46	1.72
2.2	1.53	2.08	7.13×10^{-3}	7.82×10^{-4}
2.4	1.02	1.62	3.56	3.58
2.6	7.20×10^{-3}	1.29	1.74	1.66
2.8	5.16	1.02	8.29×10^{-4}	7.79×10^{-5}
3.0	3.73	8.25×10^{-3}	3.92	3.59
3.5	1.74	4.70		
4.0	8.72×10^{-4}	2.73		
4.5	4.52	1.57		
5.0	2.51	9.70×10^{-4}		
5.5	1.46	6.04		
6.0	8.80×10^{-5}	3.82		
6.5		2.46		
7.0		1.60		

---

* For $0 \leq x \leq 0.2$ we assume Moliere's distribution function is valid. In expanded form it is

$$P_r(x) = 21.37\, x^{-1/3} - 30.79 + 66.75\, x^{5/3} - 66.99\, x^2 .$$

** For $0 \leq x \leq 0.2$ we again use Moliere's distribution function (renormalized) viz.

$$Q_r(x) = \frac{31.94\, e^{-2x/\sqrt{0.1}}}{2x/\sqrt{0.1}} + \frac{0.806}{3.25}\, e^{-2x/\sqrt{3.25}}$$

*** For $0 \leq y \leq 0.2$

$$Q_\theta(y) = \frac{3.44}{y}\, e^{-3.46\, y} .$$

TABLE XI

Distribution Functions for $E = 10\mathcal{E}$, $W = 10\mathcal{E}$. Arbitrary Normalization.

$$x = \frac{10\mathcal{E}r}{E_s}, \qquad y = \frac{10\mathcal{E}\theta}{E_s}$$

x or y	$P_r(x)$	$Q_r(x)$	$P_\theta(y)$
0			10.0
.1			7.42
.2	9.0	7.33	5.51
.3	4.5	2.5	4.24
.4	2.45	1.12	3.08
.5	1.35	6.36×10^{-1}	2.17
.6	8.7×10^{-1}	3.73	1.56
.7	5.7	2.63	1.11
.8	3.85	1.96	7.95×10^{-1}
.9	2.72	1.53	5.73
1.0	1.98	1.21	4.14
1.2	1.10	8.1×10^{-2}	2.01
1.4	6.5×10^{-2}	5.73	9.54×10^{-2}
1.6	3.85	4.13	4.29
1.8	2.35	3.13	1.96
2.0	1.53	2.33	8.80×10^{-3}
2.4	7.2×10^{-3}	1.37	1.64
2.8	3.43	8.33×10^{-3}	3.02×10^{-4}
3.2	1.75	5.28	5.40×10^{-5}
3.6	9.3×10^{-4}	3.32	
4.0	5.32	2.15	
4.5	2.77	1.30	
5.0	1.53	8.03×10^{-4}	
5.5		4.89	
6.0	5.04×10^{-5}	3.06	

TABLE XII

Distribution Functions for $E = 5\mathcal{E}$, $W = 5\mathcal{E}$. Arbitrary Normalization.

$$x = \frac{5\,\mathcal{E}\,r}{E_s}, \qquad y = \frac{5\,\mathcal{E}\,\theta}{E_s}$$

x or y	$P_r(x)$	$Q_r(x)$	$P_\theta(y)$	$Q_\theta(y)$
0	...	...	11.2	...
.1	22.6	...	8.29	26.0
.2	9.9	7.33	6.05	9.0
.3	4.7	2.5	4.37	4.2
.4	2.4	1.12	3.14	2.15
.5	1.4	6.36×10^{-1}	2.24	1.20
.6	8.0×10^{-1}	3.73	1.57	6.60×10^{-1}
.7	4.8	2.63	1.10	3.70
.8	3.3	1.96	7.7×10^{-1}	2.00
.9	2.34	1.53	5.4	1.20
1.0	1.70	1.21	3.75	7.20×10^{-2}
1.2	9.00×10^{-2}	7.87×10^{-2}	1.74	2.80
1.4	5.1	5.43	7.7×10^{-2}	1.10
1.6	3.10	3.90	3.36	4.5×10^{-3}
1.8	1.90	2.83	1.40	1.7
2.0	1.20	2.06	5.6×10^{-3}	6.7×10^{-4}
2.4	5.3×10^{-3}	1.15	7.8×10^{-4}	8.0×10^{-5}
2.8	2.50	6.57×10^{-3}	1.12	7.2×10^{-6}
3.2	1.27	3.98		
3.6	6.70×10^{-4}	2.45		
4.0	3.70	1.57		
4.5	1.88	9.17×10^{-4}		
5.0	1.05	5.35		
5.5		3.13		
6.0	3.47×10^{-5}	1.87		

TABLE XIII

Distribution Functions for $E = 2\varepsilon$. Arbitrary Normalization.

$$x = \frac{2\varepsilon r}{E_s} \qquad y = \frac{2\varepsilon\theta}{E_s}$$

x or y	$P_r(x)$	$Q_r(x)$	$P_\theta(y)$	$Q_\theta(y)$
0			11.8	
.1	23.0		9.0	29.0
.2	11.0	7.33	6.8	9.4
.3	5.6	2.5	5.1	4.0
.4	2.85	1.12	3.65	1.90
.5	1.55	6.36×10^{-1}	2.6	9.5×10^{-1}
.6	8.0×10^{-1}	3.73	1.80	5.2
.7	4.35	2.63	1.18	2.87
.8	2.30	1.96	7.1×10^{-1}	1.58
.9	1.30	1.53	4.4	8.8×10^{-2}
1.0	8.5×10^{-2}	1.21	2.70	5.0
1.2	4.0	7.67×10^{-2}	1.08	1.5
1.4	2.18	5.04	3.9×10^{-2}	4.7×10^{-3}
1.6	1.28	3.48	1.42	1.38
1.8	8.0×10^{-3}	2.37	5.0×10^{-3}	4.1×10^{-4}
2.0	5.1	1.64	1.65	1.33
2.4	2.33	8.03×10^{-3}	1.70×10^{-4}	1.15×10^{-5}
2.8	1.14	4.13	2.10×10^{-5}	1.15×10^{-6}
3.2	5.85×10^{-4}	2.18		
3.6	3.05	1.24		
4.0	1.80	7.65×10^{-4}		
4.5	9.2×10^{-5}	4.28		
5.0	4.9	2.52		

TABLE XIV

Angular Distribution of Electrons for $s = 0.6$, 1.0 and 1.5.

x	$P_\theta(x, s)$		
	$s = 0.6$	$s = 1.0$	$s = 1.5$
0	13	9.3	6.1
.1	9.1	7.1	5.0
.2	6.3	5.3	4.1
.4	3.10	2.78	2.60
.6	1.48	1.52	1.58
.8	7.10×10^{-1}	8.20×10^{-1}	9.00×10^{-1}
1.0	3.45	4.46	5.10
1.2	1.66	2.32	2.75
1.4	8.00×10^{-2}	1.18	1.50
1.6	3.80	6.00×10^{-2}	8.00×10^{-2}
1.8	1.80	2.90	4.18
2.0	8.20×10^{-3}	1.46	2.18
2.2	3.70	7.13×10^{-3}	1.12
2.4	1.58	3.56	5.60×10^{-3}
2.6	6.7×10^{-4}	1.74	2.75
2.8	2.7	8.29×10^{-4}	1.38
3.0	1.12	3.92	6.50×10^{-4}

TABLE XV

Angular Distribution of Photons for $s = 0.6$, 1.0 and 1.5.

y	$yQ_\theta(y, s)$		
	s = 0.6	s = 1.0	s = 1.5
0	4.7	3.4	2.1
.1	2.9	2.4	1.8
.2	1.8	1.7	1.5
.4	6.50×10^{-1}	8.76×10^{-1}	1.00
.6	2.61	4.61	6.42×10^{-1}
.8	1.18	2.21	3.83
1.0	5.06×10^{-2}	1.18	2.22
1.2	2.28	5.47×10^{-2}	1.19
1.4	1.03	2.74	6.28×10^{-2}
1.6	4.80×10^{-3}	1.38	3.30
1.8	2.25	6.87×10^{-3}	1.66
2.0	1.06	3.44	8.44×10^{-3}
2.2	4.83×10^{-4}	1.72	4.02
2.4	2.25	8.59×10^{-4}	1.89
2.6	1.05	4.32	8.90×10^{-4}
2.8	5.15×10^{-5}	2.18	4.12
3.0	2.43	1.07	1.91

TABLE XVI

Radial Distribution of Electrons for s = 0.6, 1.0 and 1.5.

x	$P_r(x, s)$		
	s = 0.6	s = 1.0	s = 1.5
0			
.2	11.0	7.62	5.00
.4	2.85	2.74	2.00
.6	8.00×10^{-1}	1.01	1.08
.8	2.30	4.84×10^{-1}	6.10×10^{-1}
1.0	8.50×10^{-2}	2.52	3.75
1.2	4.00	1.47	2.40
1.4	2.18	8.72×10^{-2}	1.60
1.6	1.22	5.36	1.14
1.8	7.40×10^{-3}	3.49	8.20×10^{-2}
2.0	4.50	2.26	6.00
2.2	2.90	1.53	4.50
2.4	2.00	1.02	3.50
2.6	1.37	7.20×10^{-3}	2.75
2.8	9.50×10^{-4}	5.16	2.15
3.0	6.70	3.73	1.70
3.5	3.00	1.74	9.80×10^{-3}
4.0	1.36	8.72×10^{-4}	6.00
4.5	6.20×10^{-5}	4.52	3.65
5.0	2.99	2.51	2.30
5.5	1.39	1.46	1.47
6.0	6.80×10^{-6}	8.80×10^{-5}	9.80×10^{-4}
7.0	1.58		4.70×10^{-4}
8.0			2.40
9.0			1.33

FIGURE CAPTIONS

Figure 1. Angular moments for electron distribution function vs. depth (parameter s).

Figure 2. Angular moments for photon distribution function vs. depth (parameter s).

Figure 3. Radial moments for electron distribution function vs. depth (parameter s).

Figure 4. Angular distribution function at shower maximum for electrons plotted for several energies.

Figure 5. Radial distribution function at shower maximum for photons plotted for several energies.

Figure 6. Radial distribution function at shower maximum for electrons plotted for several energies.

Figure 7. Angular distribution function of electrons as a function of depth (Approximation A).

Figure 8. Angular distribution function of photons as a function of depth (Approximation A).

Figure 9: Radial distribution function of electrons as a function of depth (Approximation A).

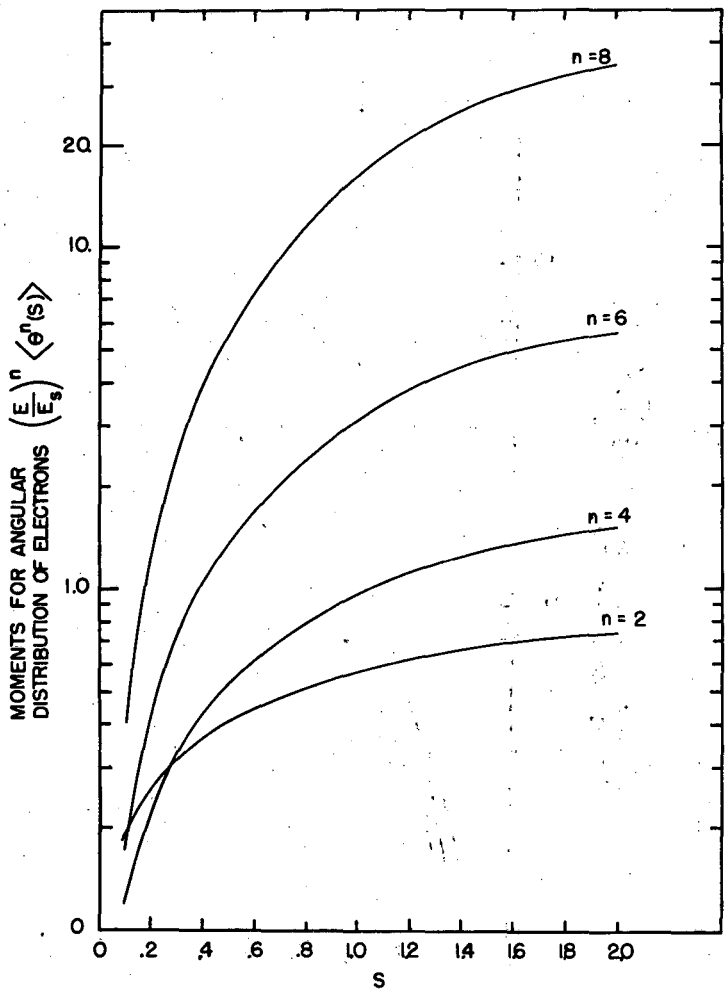

FIG. 1 - SECTION II

MU 2082

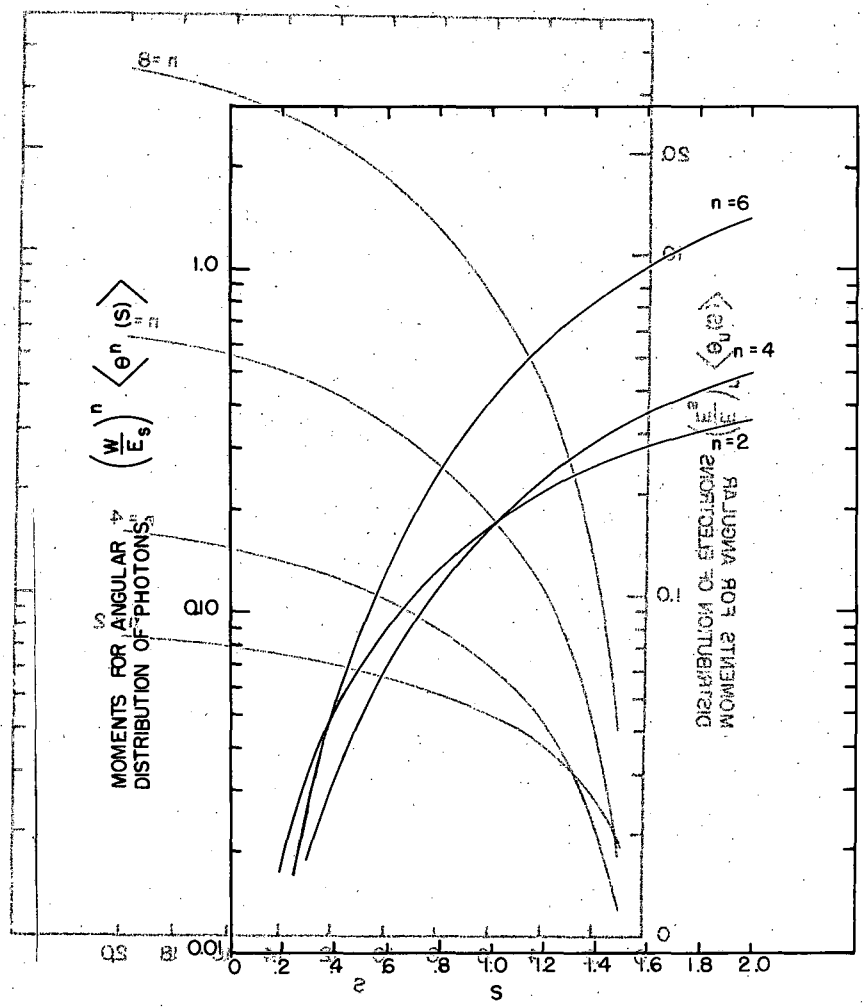

FIG. 2 - SECTION II

MU 2083

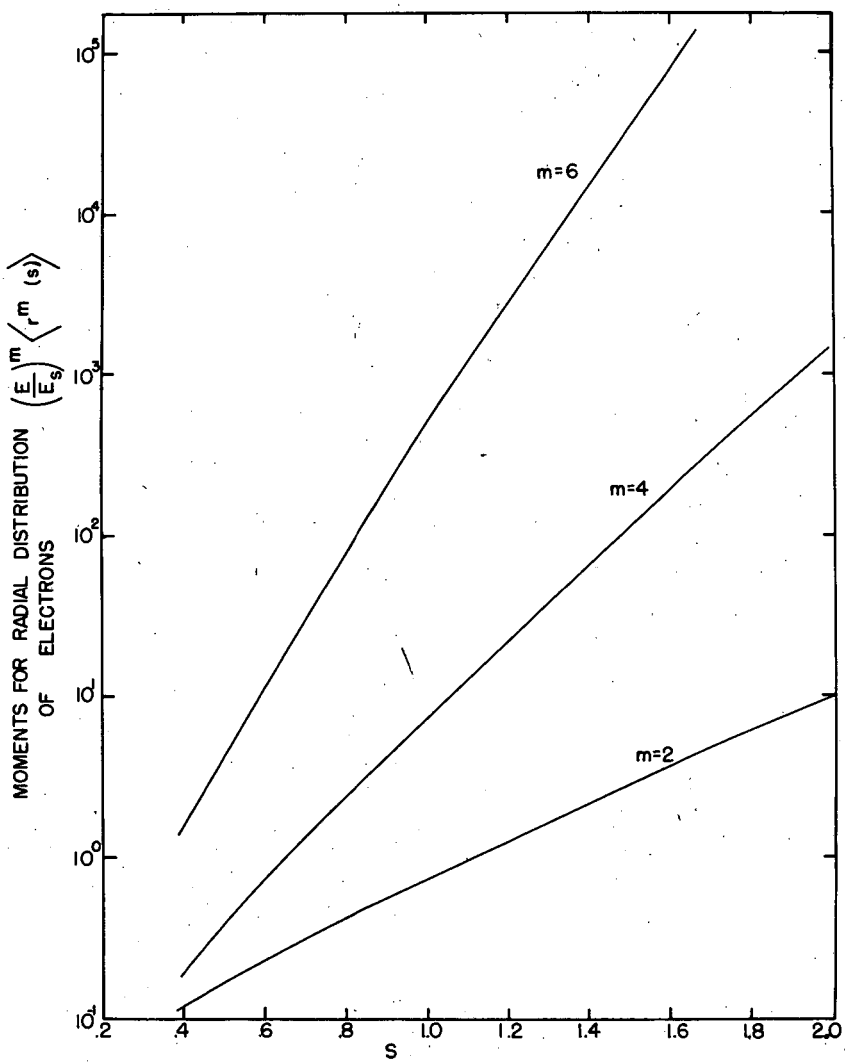

FIG. 3 - SECTION II

MU 2084

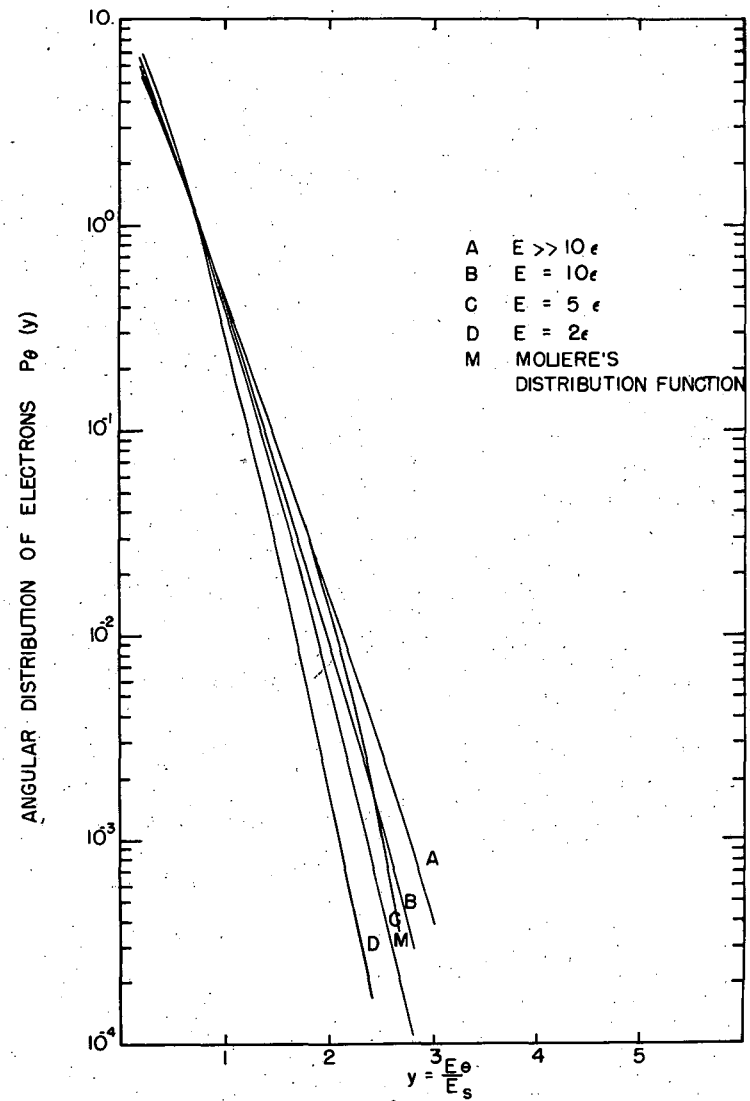

FIG. 4 — SECTION II MU 2085

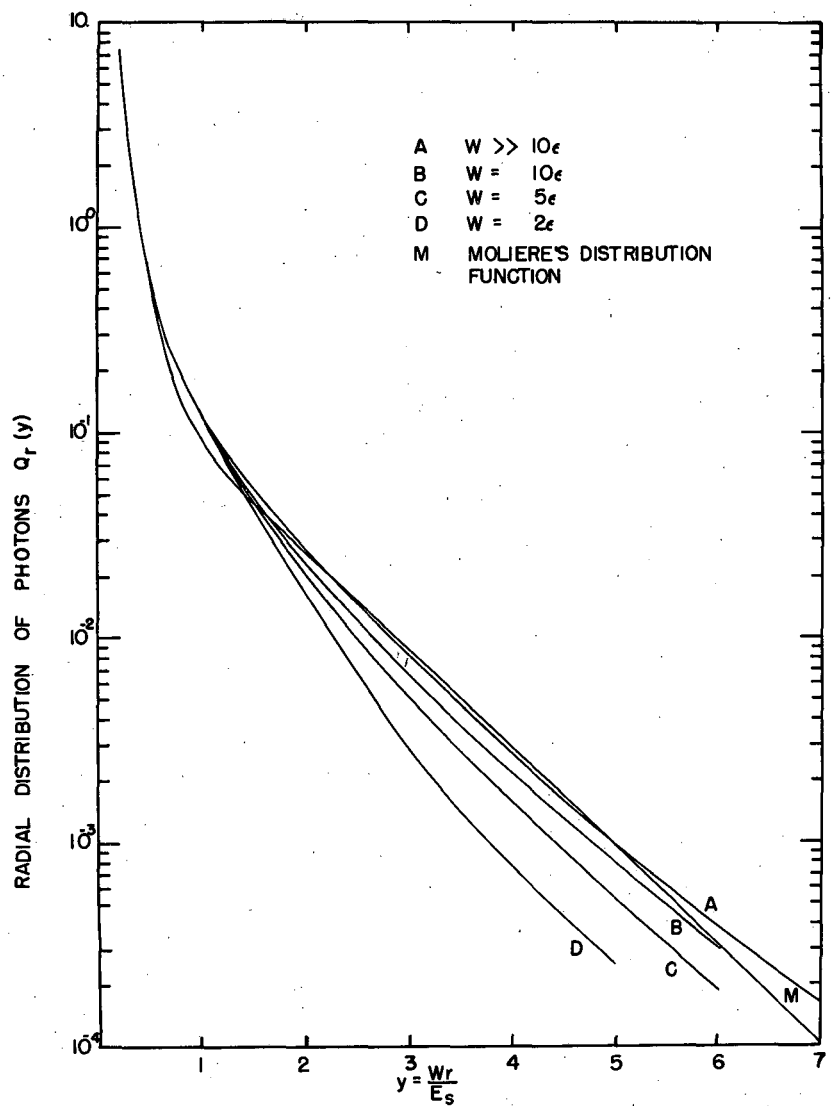

FIG. 5 - SECTION II MU 2086

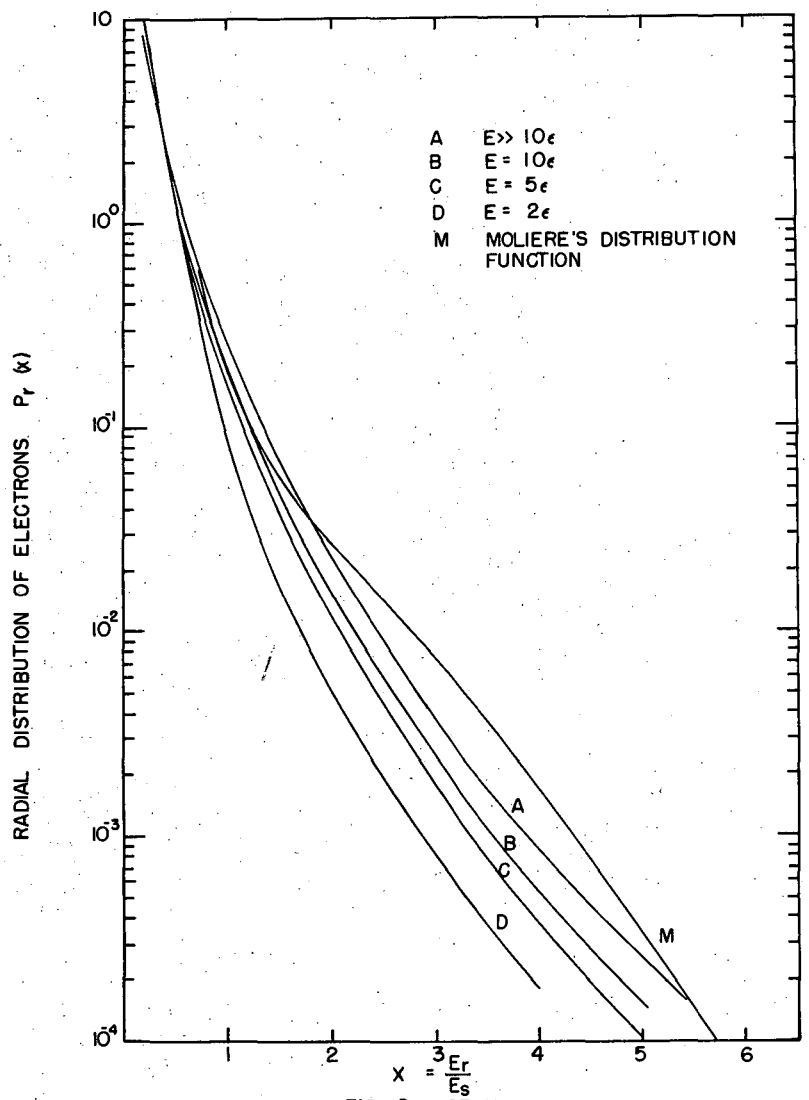

FIG. 6 - SECTION II

MU 2087

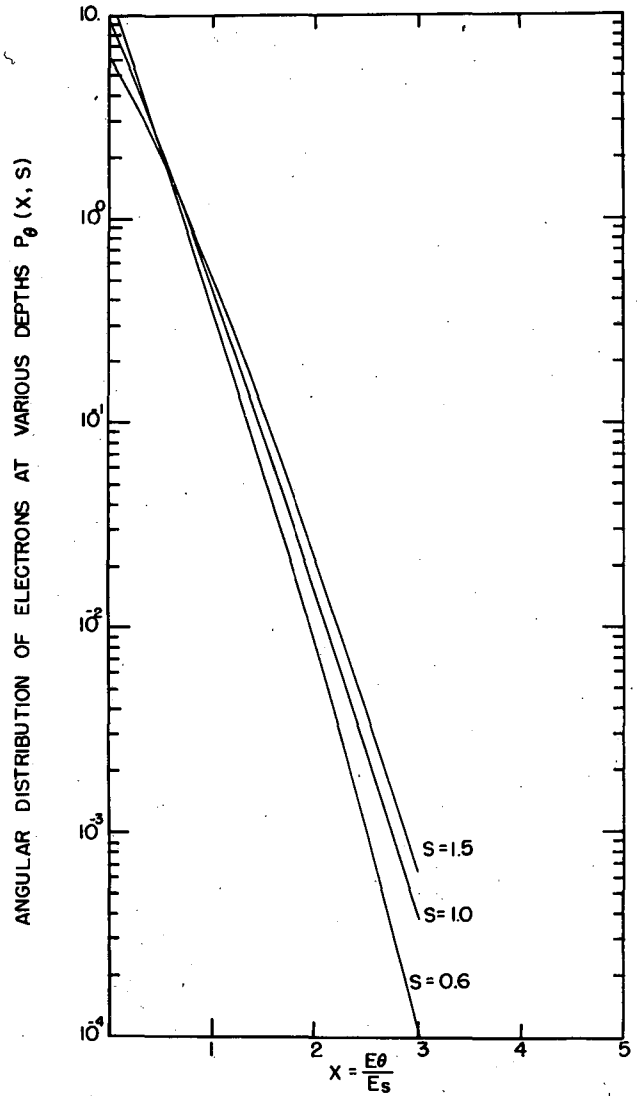

FIG. 7 – SECTION II MU 2088

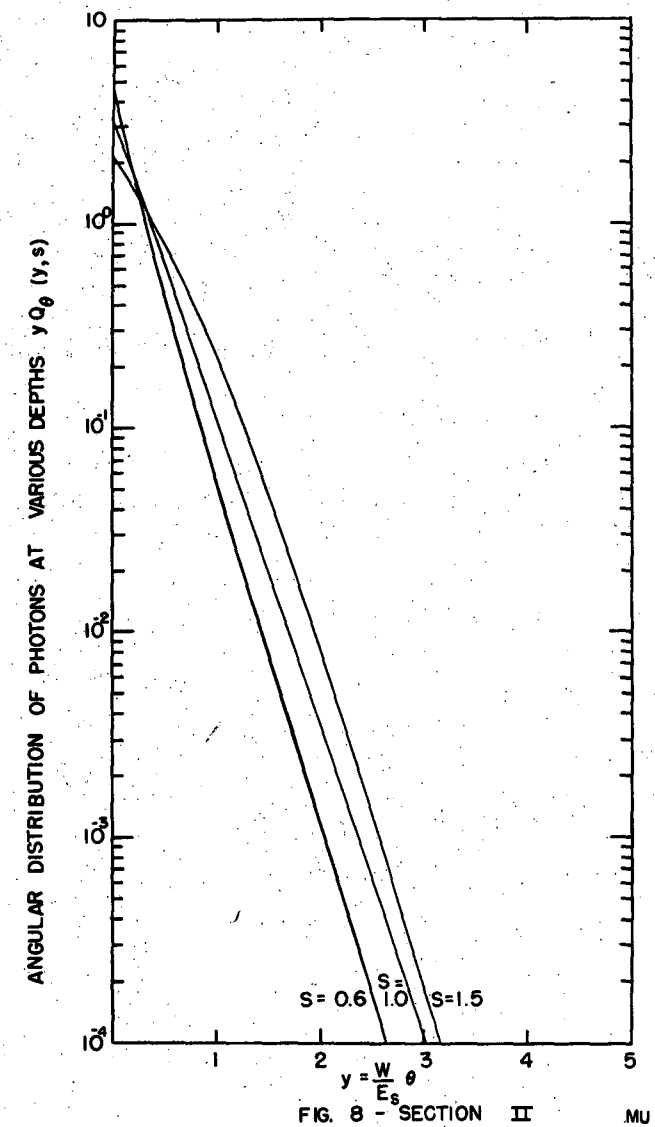

FIG. 8 - SECTION II

MU 2089

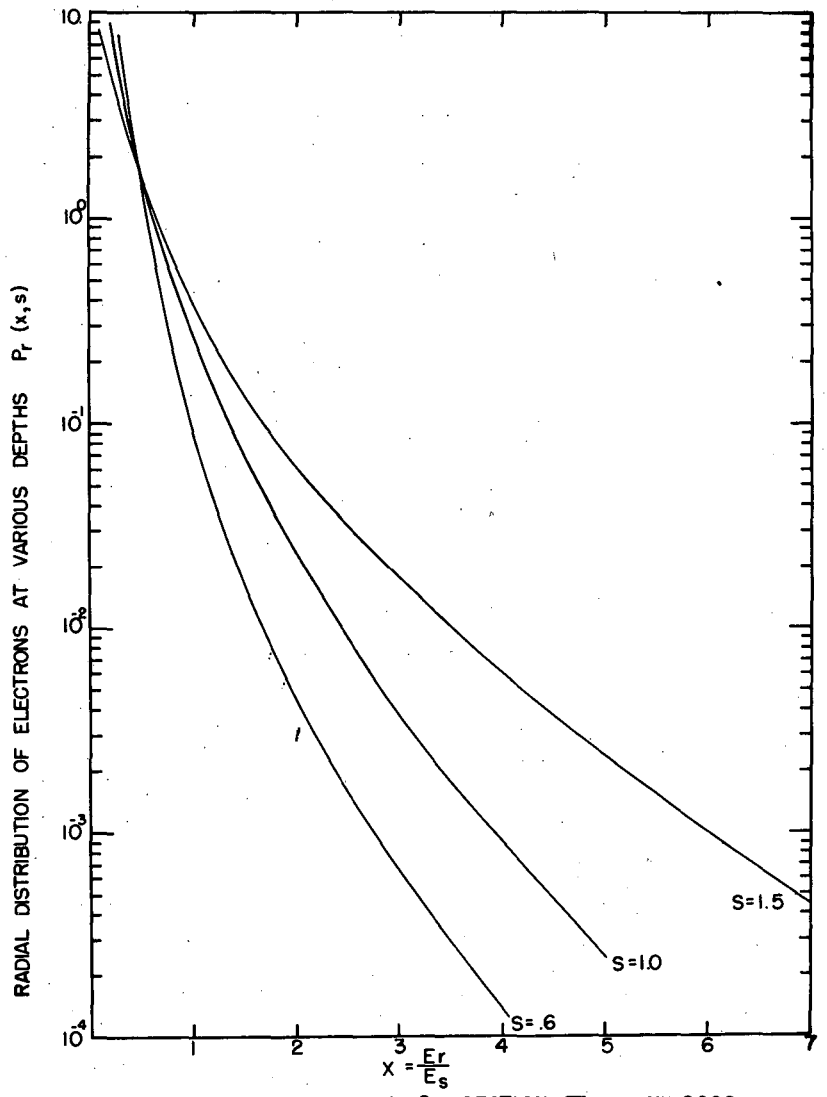

FIG. 9 - SECTION II MU 2090

ACKNOWLEDGMENTS

The work described in the first section on scattering of high energy neutrons was done in collaboration with T. B. Taylor under the guidance of Professor Robert Serber, who suggested the problem.

The study of cosmic-ray showers in the second section was suggested By Dr. L. Eyges and was carried out with his assistance and under his direction.

It is a pleasure to thank Professor Serber, who was extremely helpful throughout the course of the work and Professor W. A. Nierenberg who was kind enough to read and critize the manuscript.

All the work described in this paper was performed under the auspices of the Atomic Energy Commission.